Multiplexed Photoionization Mass Spectrometry Investigation of the O(3 P) + Propyne Reaction

ARTICLE *in* THE JOURNAL OF PHYSICAL CHEMISTRY A · MAY 2015

Impact Factor: 2.69 · DOI: 10.1021/acs.jpca.5b00491 · Source: PubMed

6 AUTHORS, INCLUDING:

John D Savee

Los Gatos Research

49 PUBLICATIONS **668** CITATIONS

SEE PROFILE

Oliver Welz

BASF SE

46 PUBLICATIONS **677** CITATIONS

SEE PROFILE

Craig A Taatjes

Sandia National Laboratories

200 PUBLICATIONS **4,489** CITATIONS

SEE PROFILE

David Osborn

Sandia National Laboratories

126 PUBLICATIONS **2,353** CITATIONS

SEE PROFILE

THE JOURNAL OF PHYSICAL CHEMISTRY A

Article

pubs.acs.org/JPCA

Multiplexed Photoionization Mass Spectrometry Investigation of the O(^{3}P) + Propyne Reaction

John D. Savee,[†] Sampada Borkar,[‡] Oliver Welz,[†,§] Bálint Sztáray,[‡] Craig A. Taatjes,[†] and David L. Osborn*[,†]

[†]Combustion Research Facility, Sandia National Laboratories, Mail Stop 9055, Livermore, California 94551-0969, United States

[‡]Department of Chemistry, University of the Pacific, Stockton, California 95211, United States

Supporting Information

ABSTRACT: The reaction of O(^{3}P) + propyne (C_3H_4) was investigated at 298 K and 4 Torr using time-resolved multiplexed photoionization mass spectrometry and a synchrotron-generated tunable vacuum ultraviolet light source. The time-resolved mass spectra of the observed products suggest five major channels under our conditions: C_2H_3 + HCO, CH_3 + HCCO, H + CH_3CCO, C_2H_4 + CO, and C_2H_2 + H_2 + CO. The relative branching ratios for these channels were found to be 1.00, (0.35 ± 0.11), (0.18 ± 0.10), (0.73 ± 0.27), and (1.31 ± 0.62). In addition, we observed signals consistent with minor production of C_3H_3 + OH and H_2 + CH_2CCO, although we cannot conclusively assign them as direct product channels from O(^{3}P) + propyne. The direct abstraction mechanism plays only a minor role (≤1%), and we estimate that O(^{3}P) addition to the central carbon of propyne accounts for 10% of products, with addition to the terminal carbon accounting for the remaining 89%. The isotopologues observed in experiments using d_1-propyne (CH_3CCD) and analysis of product branching in light of previously computed stationary points on the singlet and triplet potential energy surfaces (PESs) relevant to O(^{3}P) + propyne suggest that, under our conditions, (84 ± 14)% of the observed product channels from O(^{3}P) + propyne result from intersystem crossing from the initial triplet PES to the lower-lying singlet PES.

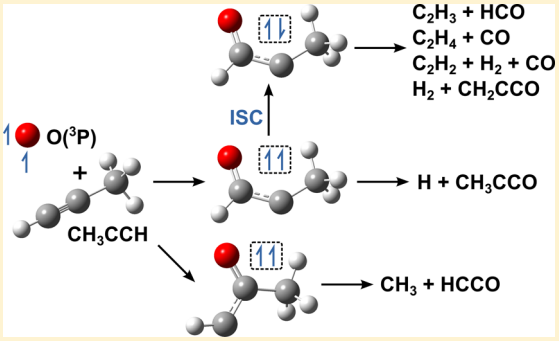

1. INTRODUCTION

The ground-state oxygen atom, O(^{3}P), is readily produced in combustion environments by the H + O_2 reaction and is a critical oxidizer of hydrocarbons.[1] Not surprisingly, reactions of O(^{3}P) with various hydrocarbons have received considerable attention, particularly the cases where O(^{3}P) reacts with unsaturated hydrocarbon species that often result in complex multichannel reaction pathways. The influential reviews on this subject by Cvetanovic[2,3] summarized several decades of work and formulated general trends by which these reactions occur. Two main conclusions are that electrophilic O(^{3}P) addition dominates H-atom abstraction at low temperature and addition preferentially occurs at the less-substituted carbon atom of the multiple bond.

Compared to the reaction of a doublet radical with a closed shell hydrocarbon, which proceeds on a doublet potential energy surface (PES), the addition of O(^{3}P) to a singlet species explores a much more diverse landscape; bimolecular products may be two singlets, two triplets, triplet + singlet, or two doublets. Thus, at least at low pressure, reactions of O(^{3}P) with smaller alkenes and alkynes typically proceed via several bimolecular product channels in which both stable and transient species are produced, and versatile experiments capable of monitoring all reaction products are desirable to reveal the underlying reaction mechanisms.

Early experiments studying these reactions were limited to end-product analysis of stable species or time-resolved studies of a limited number of transient (i.e., free radical) or stable products. Recent advances combining crossed molecular beams (CMBs) and novel mass spectrometry techniques have allowed new insight into several fundamental cases of O(^{3}P) reacting with an unsaturated hydrocarbon, most notably the reactions with acetylene (C_2H_2),[4,5] ethene (C_2H_4),[6−8] and allene (CH_2=C=CH_2, C_3H_4)[9] in single collision environments. An account of two of the reaction channels of O(^{3}P) with propyne (HC≡C−CH_3, another isomer of C_3H_4) has been recently reported.[10] These CMB experiments using soft electron-impact ionization are advantageous because they allow "universal" detection of nearly all products of these reactions. The measured product branching fractions, together with high-level quantum chemical calculations[11−13] and more recently with quasi-classical trajectory calculations,[14−17] have shown that

Special Issue: 100 Years of Combustion Kinetics at Argonne: A Festschrift for Lawrence B. Harding, Joe V. Michael, and Albert F. Wagner

Received: January 16, 2015
Revised: April 29, 2015
Published: May 18, 2015

DOI: 10.1021/acs.jpca.5b00491
J. Phys. Chem. A 2015, 119, 7388−7403

these reactions are subject to significant intersystem crossing (ISC) from the initial triplet PES of the adduct to the singlet PES en route to product formation. Quantum mechanical treatments of non-adiabatic ISC dynamics are difficult, as they require accurate knowledge of the location and coupling strengths where the triplet and singlet PESs interact. Thus, accurate quantitative experimental observables for these reactions are of critical importance in the development of predictive theoretical methods for this reaction class.

Recently we have shown that time- and isomer-resolved accounts of chemical reactions obtained from experiments using multiplexed synchrotron photoionization mass spectrometry (MPIMS) coupled to a photolytic flow reactor are an illuminating probe of reactions of $O(^3P)$ with prototypical unsaturated hydrocarbons.[18,19] Similar to CMB experiments, MPIMS uses soft ionization (here, VUV synchrotron radiation) to observe nearly all products from a chemical reaction. The results from MPIMS studies of $O(^3P)$ with propene (CH_3–$CH{=}CH_2$, C_3H_6) yielded quantitative determinations of the site-specificity for the initial $O(^3P)$ attack, details of a previously unobserved H_2-loss channel, and evidence that up to 40% of the observed products occur after ISC at 298 K and 4 Torr.[19] By comparison, CMB studies of $O(^3P)$ + allene (C_3H_4, $CH_2{=}C{=}CH_2$), another unsaturated three-carbon species, indicated that ISC accounts for over 90% of the observed products.[9]

Our current work presents an in-depth investigation into the reaction of $O(^3P)$ with propyne (R1), an isomer of allene and the smallest alkyne with two distinct carbon atom sites (C_1 vs C_2) to which $O(^3P)$ can add.

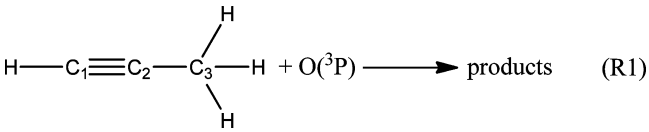

(R1)

Propyne is also of considerable interest as a methyl-substituted analogue of acetylene; electronically it is quite similar to acetylene, although propyne has many more vibrational degrees of freedom that may influence the competition between dissociation and ISC on the triplet PES. Recent RRKM/master equation calculations[11] and direct dynamics studies[16] have found that experimentally observed product yields (see ref 4 and references therein) from $O(^3P)$ + acetylene at modest collision energies (<13 kcal/mol) are consistent with only minor contributions from ISC (<10% of all product formation), although to date no conclusive experimental evidence exists for products resulting from ISC. This minor involvement of ISC in the reaction of $O(^3P)$ with acetylene, contrasting with the large degree of ISC in the reaction with the C_3H_4 isomer allene, makes propyne an interesting case study for identifying ISC trends in $O(^3P)$ + hydrocarbon reactions.

The present study builds on several previous investigations of R1. Of particular interest, Kanofsky et al. used high-density CMB experiments coupled with photoionization mass spectrometry detection to provide a broad survey of the products of R1.[20] Signal intensities of observed products using photoionization energies accessible by a variety of discharge lamps were consistent with several major (R1a–R1d, R1g) and minor (R1e/R1e′, R1f) product channels.

$$CH_3CCH + O(^3P) \rightarrow C_2H_3 + HCO \quad (\Delta H_{rxn} = -19.0 \text{ kcal/mol}) \quad \text{(R1a)}$$

$$\rightarrow CH_3 + HCCO \quad (\Delta H_{rxn} = -22.1 \text{ kcal/mol}) \quad \text{(R1b)}$$

$$\rightarrow CH_3CCO + H \quad (\Delta H_{rxn} = -13.4 \text{ kcal/mol}) \quad \text{(R1c)}$$

$$\rightarrow C_2H_4 + CO \quad (\Delta H_{rxn} = -115.1 \text{ kcal/mol}) \quad \text{(R1d)}$$

$$\rightarrow C_2H_2 + H_2 + CO \quad (\Delta H_{rxn} = -76.7 \text{ kcal/mol}) \quad \text{(R1e)}$$

$$\rightarrow C_2H_2 + H_2CO \quad (\Delta H_{rxn} = -73.4 \text{ kcal/mol}) \quad \text{(R1e′)}$$

$$\rightarrow C_3H_3 + OH \quad (\Delta H_{rxn} = -4.4 \text{ kcal/mol}) \quad \text{(R1f)}$$

$$\rightarrow C_2H_2O + CH_2 \quad (\Delta H_{rxn} = -19.6 \text{ kcal/mol}) \quad \text{(R1g)}$$

Reported energetics are at 0 K based on calculations by Zhao et al.[21] (except that for R1e′ which comes from calculations in ref 22). In the experiments by Kanofsky et al., partially deuterated propyne precursors were used, and the isotopologue yields for products of R1c support that methylketenyl (CH_3CCO) is the major C_3H_3O isomer formed. In recent CMB experiments, Balucani et al. explored channels R1b and R1c, and reported that R1b is favored over R1c by a factor of 3.1 ± 0.6.[10] Variations of channel R1d in which energetic forms of C_2H_4 are produced (e.g., the $^3CH_3CH$ ethylidene isomer) are energetically possible and are discussed in more detail later.

Other product channels resulting from R1, such as loss of H_2 (R1h), are also energetically possible[21] but were not observed by Kanofsky et al. and are observed with only a minor yield by Balucani et al.[10]

$$CH_3CCH + O(^3P) \rightarrow CH_2CCO + H_2 \quad (\Delta H_{rxn} = -66.5 \text{ kcal/mol}) \quad \text{(R1h)}$$

The CMB studies in ref 20 utilized dense molecular beams, and although they nominally produce only primary products of R1, there is some evidence that secondary or side reaction products are also formed in such experiments.[19] The MPIMS experiments in the present work have a temporal resolution sufficient to discriminate between primary and secondary chemistry and also the sensitivity to detect minor channels such as H_2-loss (e.g., R1h). These reasons, coupled with the ability to generate quantitative accounts of product branching, provided an impetus to reinvestigate R1. In addition, the use of tunable synchrotron VUV radiation as the ionization source in MPIMS experiments enables unambiguous identification of the isomeric composition of many products.

DOI: 10.1021/acs.jpca.5b00491
J. Phys. Chem. A 2015, 119, 7388–7403

2. EXPERIMENT

The working principles of time-resolved MPIMS experiments have been described in detail elsewhere.[23−25] The experiments were performed at 298 K using a quartz flow reactor in which a mixture of propyne (or d_1-propyne, CH_3CCD), NO_2, and helium were introduced via calibrated mass flow controllers. The pressure inside the quartz reactor was maintained at 4 Torr by throttling the outflow to a vacuum pump. R1 was initiated by a 351 nm pulse from an excimer laser (i.e., by photodissociating NO_2 to $O(^3P)$ + NO), and the contents of the reactor were continuously sampled through a ∼650 μm aperture in the side wall. The bulk velocity of the gas flow was ∼1000 cm/s to ensure that a fresh gas sample was present in the reactor at the time of photolysis when signal averaging at a 10 Hz repetition rate of the excimer laser. The near-effusive molecular beam of sampled products was then skimmed and crossed by monochromatized tunable synchrotron-generated VUV radiation (∼30 meV fwhm) from the Chemical Dynamics Beamline[26,27] at the Advanced Light Source of Lawrence Berkeley National Laboratory or by the VUV spectrum emitted by a hollow-cathode hydrogen discharge lamp with a MgF_2 window (emitting photons <11 eV). Cations generated by photoionization were electrostatically focused and extracted at 50 kHz into an orthogonal acceleration time-of-flight mass spectrometer coupled to a time-sensitive microchannel plate detector. The mass resolution of the mass spectrometer ($m/\Delta m \approx 1500$) is sufficient to assign the sum formulas of the products, e.g., to discriminate between C_2H_5 vs HCO at m/z = 29. The time-of-flight (yielding mass-to-charge ratio m/z), kinetic time relative to the photolysis pulse (t), and photoionization energy (E) for detected events were recorded using a transient digitizer with fundamental time bins of 250 ps. The presented data [i.e., $I(m/z,t)$ at a single photoionization energy or $I(m/z,t,E)$ if the photoionization energy is scanned] are background subtracted using 10 ms of pre-photolysis signal so that intensity represents the *change* in signal after photolysis. Moreover, presented data from photoionization scans are normalized to the photon flux measured by a calibrated photodiode (SXUV-100, International Radiation Detectors, Inc.) at each photoionization energy step.

Reported total rate coefficients for R1 near 298 K and at low pressure (<10 Torr) range from $\sim 7.1 \times 10^{-13}$ to 8.6×10^{-13} $cm^3\ s^{-1}$.[28−31] In the following discussion, we use a value of $k_1 = 7.4 \times 10^{-13}\ cm^3\ s^{-1}$ evaluated in a review by Cvetanovic.[3] The competing $O(^3P) + NO_2$ reaction has a rate coefficient of $k_0 \approx 1.0 \times 10^{-11}\ cm^3\ s^{-1}$.[32,33] Except where indicated, experiments were performed with $[propyne]_0 \approx 1.9 \times 10^{15}\ cm^{-3}$ and $[NO_2]_0 \approx 1.0 \times 10^{13}\ cm^{-3}$, which, under pseudo-first-order conditions, will deplete $O(^3P)$ with a pseudo-first-order rate coefficient of ∼1500 s^{-1} (i.e., $k_1[propyne]_0 + k_0[NO_2]_0$ and neglecting heterogeneous wall loss of $O(^3P)$), keeping the reaction of $O(^3P)$ with propyne ∼14 times more likely than reaction with NO_2. Direct products of R1 are kinetically linked to the decay of $O(^3P)$ and should therefore have formation rates of ∼1500 s^{-1}. The typical output of the photolysis laser is ∼39 mJ cm^{-2} $pulse^{-1}$ at 351 nm and by using the known photoabsorption cross-section of NO_2 ($\sim 4.8 \times 10^{-19}\ cm^2$ near 298 K) and a quantum yield of unity for $O(^3P)$ + NO formation we estimate ∼3.3% of the NO_2 is photodissociated yielding $[O(^3P)]_0 \approx 3.4 \times 10^{11}\ cm^{-3}$.[34,35]

Photoionization energy scans provide isomer-resolved identification of products. In a recent investigation into the reaction of $O(^3P)$ with propene,[19] which is ∼6 times faster than R1, reactant concentrations could be maintained sufficiently low so that photoionization scans used for both product identification and quantification could be extended above the adiabatic ionization energy (AIE) of propene at 9.73 eV.[36] However, the large concentration of propyne required in the present experiments, coupled with its unusually large near-threshold photoionization cross-section, led to a large background signal above the AIE of propyne at 10.36 eV[36] inhibiting our ability to scan above this energy with useful signal-to-noise ratios. Approximately 2×10^3 repetitions of the experiment at each photoionization energy were averaged to produce the photoionization energy scan data given in the present work.

Identification and quantification of species with higher AIEs such as ethene (m/z = 28, AIE = 10.51 eV)[36] and acetylene (m/z = 26, AIE = 11.40 eV)[36] were performed using selected single photoionization energies (near 10.2, 10.8, and 11.5 eV), with much longer signal averaging than would be possible in a photoionization energy scan (approximately $(5−10) \times 10^4$ repetitions in synchrotron experiments and 3×10^5 repetitions when using the H_2 lamp). These single energy measurements were also used to fit product time profiles to a pseudo-first-order kinetics model of parallel sequential reactions (see the Supporting Information) providing formation and decay rate coefficients and signal levels for the fitted data.

Relative branching ratios for various product channels (i.e., N_i/N_j) can be determined from extracted signal for representative species if the isomeric yield, absolute photoionization cross-sections for the individual isomers, and the instrumental mass discrimination are known.[19,23,24,37] Under the assumption that all product channels of R1 are observed, branching ratios can then be converted into branching fractions (i.e., $N_i/\sum_j N_j$) for the reaction.

Absolute photoionization cross-sections for acetylene, ethene, ketene, and nitric oxide were measured using the methods described in ref 38 and are reported in the Supporting Information. In cases where experimental measurements or previously calculated stationary point energies for R1 were not available, quantum chemical calculations were performed using the CBS-QB3 method[39,40] within the Gaussian09[41] suite of programs to guide interpretation of experimental observations.

3. RESULTS

In photoionization scans of R1 between 8.209 and 10.309 eV, significant time-resolved signals were observed at m/z = 15, 27, 29, 30, 39, 41, 42, 54, and 55. Careful calibration of the time-of-flight mass spectrometer allows determination that m/z = 15 is CH_3, m/z = 27 is C_2H_3, m/z = 29 is a major HCO product and a minor C_2H_5 product, m/z = 39 is C_3H_3, m/z = 41 is both C_3H_5 and HCCO, m/z = 42 is C_2H_2O, m/z = 54 is C_3H_2O, and m/z = 55 is C_3H_3O. Identification of the isomeric composition of many of these products is performed using measured photoionization spectra as discussed below. From single-energy experiments at higher photoionization energies, additional products were observed at m/z = 28 (C_2H_4, observed at 10.8 and 11.5 eV) and m/z = 26 (C_2H_2, observed only at 11.5 eV). Formaldehyde is a potential product at m/z = 30 (from R1e′) that can in principle be detected above its AIE (10.88 eV),[36] but was not observable in the present experiments due to contamination from a large NO signal (also at nominal m/z = 30 with AIE = 9.26 eV),[36] which arises from photolysis of NO_2. However, d_1-formaldehyde was

DOI: 10.1021/acs.jpca.5b00491
J. Phys. Chem. A 2015, 119, 7388−7403

Table 1. Branching Ratios and Fractions from the Present Measurements of Products Resulting from $O(^3P)$ + Propyne at 4 Torr and 298 K[a]

product channel	branching ratio relative to C_2H_3 + HCO	total branching fraction, present work	branching ratios previous work	$O(^3P)$ + allene branching fraction[g]
(C_2H_3) + (HCO) (R1a)	1.00	0.28 ± 0.05	–	0.07
(CH_3) + (HCCO) (R1b)	0.35 ± 0.11	0.10 ± 0.03	$N_{methyl}/N_{methylketenyl}$ = (3.1 ± 0.6)[e]	–
(CH_3CCO) + H (R1c)	0.18 ± 0.10	0.05 ± 0.03		0.016[h]
(C_2H_4) + CO (R1d)	0.73 ± 0.27	0.20 ± 0.07 (0.37 ± 0.09)[d]	$N_{acetylene}/N_{ethene} \approx 2$[f]	0.815
(C_2H_2) + CO + H_2 (R1e)	1.31 ± 0.62	0.36 ± 0.11 (0.19 ± 0.04)[d]		0.096
(C_3H_3)[b] + OH (R1f)	0.04 ± 0.02	0.01 ± 0.007	0[e]	–
(CH_2CCO)[b] + H_2 (R1h)	0.005 ± 0.002	<0.01	–	–
(CH_2CO)[c] + CH_2 (R1g)	0.18 ± 0.04	–	–	0.003

[a]Observed products are enclosed in parentheses, and the assumptions that were used to calculate branching fractions are outlined in the main text. Branching ratios from previous investigations of R1 are included, along with branching fractions for products of the $O(^3P)$ + allene reaction as reported in ref 9. [b]Possible secondary reaction product. [c]Determined to be a secondary reaction product. [d]Estimated flux through pathway on the C_3H_4O PES using the 600 Torr ("high-pressure") $N_{acetylene}/N_{ethene}$ yield reported in ref 58; see text for details. [e]Ref 10. [f]From gas chromatography experiments of R1 near 4 Torr, as reported in ref 58. [g]From CMB experiments as reported in ref 9. [h]C_3H_3O isomer accompanied by H-loss, identified as CH_2CCHO.

observed (m/z = 31) when d_1-propyne is used, but is assigned as mainly a secondary product. No products were observed at m/z = 56 corresponding to stabilized C_3H_4O isomers, although this channel may become significant at higher pressures where collisional stabilization becomes more effective.

This section begins with a description of how these observed reaction products were assigned to primary products of R1 or to secondary or side reactions, followed by in-depth analysis of the isomeric composition and quantification of the primary reaction products. The results from d_1-propyne experiments are more complicated and will be discussed with regards to individual product channels. Table 1 presents the branching ratios measured here and their conversion to total branching fractions under assumptions summarized at the beginning of section 4, where we also discuss how these values provide evidence for the active dynamical processes on the underlying triplet and singlet C_3H_4O PESs that govern R1.

3.1. Primary vs Secondary Product Formation. The observed C_2H_5 and C_3H_5 species clearly arise from secondary chemistry because these products have more hydrogen atoms than propyne, and can be excluded from further consideration as primary reaction products. The other observed products are consistent with the observations of Kanofsky et al.,[20] with the addition of weak C_3H_2O signal that may arise from a minor R1h channel.

A high signal-to-noise time-resolved data set was obtained using a hydrogen discharge lamp as the VUV photoionization source allowing the observation of CH_3, C_2H_3, C_2H_4, HCO, C_2H_5, C_3H_3, C_2H_2O, C_3H_2O, and C_3H_3O. Propyne is also ionized using this discharge lamp, and large signal from the single ^{13}C isotopologue of propyne at m/z = 41 obscured any potential time-resolved signal from C_3H_5 or HCCO. Time profiles for the transient products observed at m/z = 15 (CH_3), 27 (C_2H_3), and 55 (C_3H_3O) are shown in Figure 1a. Formation rates in excess of the anticipated value of ~1500 s^{-1} (see section 2 and the Supporting Information) were determined for all three species, which, considering additional wall loss of $O(^3P)$, are consistent with direct products of R1. The low signal-to-noise for the transient m/z = 39 (C_3H_3) product yielded large uncertainties in its fitted formation rate, making it difficult to assign it as a result of primary or secondary chemistry.

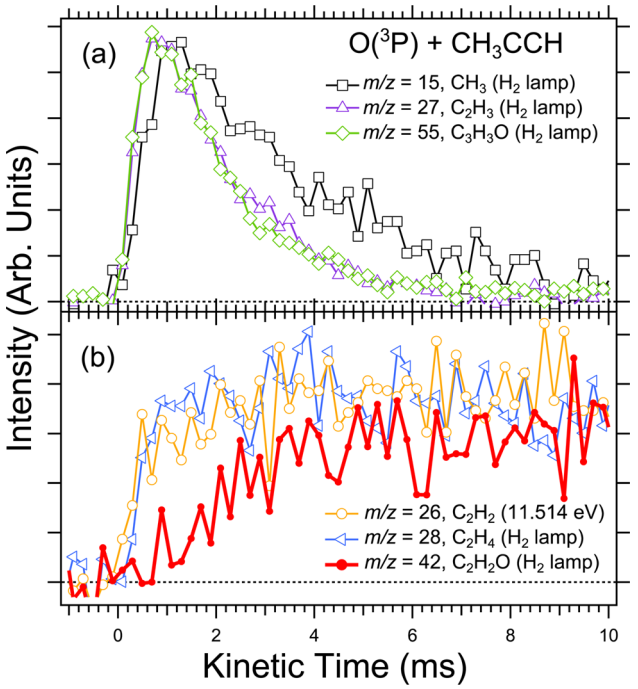

Figure 1. Time profiles for various (a) transient and (b) stable products observed in the reaction of $O(^3P)$ with propyne. All data were obtained using a hydrogen lamp as an ionization source except for m/z = 26, which was obtained using 11.514 eV synchrotron radiation. Time profiles of all species, arbitrarily scaled in intensity for comparison, are consistent with direct production from R1, except m/z = 42 (red trace, consistent with ketene).

Time profiles for the stable species m/z = 28 (C_2H_4) and 42 (C_2H_2O) from hydrogen lamp experiments are shown in Figure 1b, along with m/z = 26 (C_2H_2) obtained using monochromatic 11.514 eV synchrotron radiation. Fits of time-dependent data to a pseudo-first-order kinetics model of parallel sequential reactions show that the formation rates of C_2H_2 and C_2H_4 are consistent with primary production from reaction of R1 (i.e., >1500 s^{-1}, see Supporting Information). A similar fit to C_2H_2O yields a formation rate of (480 ± 100) s^{-1}, clearly slower than expected for a direct product. We therefore conclude that C_2H_2O (identified as ketene, see Supporting Information) is mostly formed via secondary chemistry. The

DOI: 10.1021/acs.jpca.5b00491
J. Phys. Chem. A 2015, 119, 7388−7403

potential $^3CH_2$ or $^1CH_2$ coproducts of C_2H_2O from R1g (AIE ≈ 10.40 and 10.01 eV, respectively)[36,42] were not observed, providing no evidence for R1g in the present experiments. Kanofsky et al.[20] reported a major yield of CH_2 and C_2H_2O from R1 in their CMB study although, as was concluded in the case of $O(^3P)$ + propene, those experiments may include some product formation via secondary chemistry.[19,43] Balucani et al. reported a minor yield of CH_2 in CMB experiments at 9.2 kcal/mol collision energy,[10] and it is possible that the ketene signal observed here contains minor unresolvable contributions from primary production via R1g.

Kinetics data for the C_3H_2O product that potentially comes from R1h could not be obtained with the signal-to-noise necessary to assign it as a primary or secondary product. Although noisy, the signal for this product persists at later times and is consistent with a stable closed-shell species as discussed in section 3.8.

Additional discussion of potential sources of secondary chemistry is included in the Supporting Information, whereas the following sections focus on the identification and quantification of primary reaction products.

3.2. Channel R1a: C_2H_3 (m/z = 27) + HCO (m/z = 29). In photoionization scans of R1, a time-resolved signal that decays over ~10 ms was observed at m/z = 27 (C_2H_3) and 29 (HCO), consistent with the formation of both radical products of channel R1a that, like all other radical products observed here, are formed by reaction of $O(^3P)$ + propyne and later consumed via secondary reactions. The photoionization spectrum for m/z = 27 between 8.209 and 10.309 eV from data integrated between 0 and 10 ms after photolysis is shown as open black circles in Figure 2a. The observed spectrum is well-represented by the photoionization spectrum of the vinyl radical (AIE = 8.51 eV),[44,45] shown as a red trace in Figure 2a, supporting that only the vinyl radical contributes to m/z = 27 signal through 10.309 eV. Because the dissociation energy for vinyl to H + C_2H_2 (D_0 = 34 kcal/mol)[46] is substantially larger than the exothermicity of R1a (~ −19 kcal/mol),[21] decomposition of vinyl formed from R1 is unimportant at 298 K. In addition, formation of vinyl from decomposition of hot C_2H_4 formed in channel R1g is not likely (see Supporting Information). On the other hand, the HCO radical may not be a suitable quantitative indicator for R1a because the exothermicity of R1a[21] exceeds the energy required for HCO to decompose to H + CO (D_0 ≈ 14.5 kcal/mol).[47,48]

The observed vinyl signal is therefore the better choice to quantify R1a. Because of the strong signal and a known photoionization cross-section for the vinyl radical[44] we use it as our reference for obtaining relative yields for other products (i.e., N_i/N_{vinyl}). From these yields channel-specific branching ratios are determined for R1 as described in section 2 and further discussed in section 4.

Because we need to quantify ethene (C_2H_4) signal relative to the vinyl radical at 10.814 eV (see section 3.5), which exceeds the maximum energy of 10.309 eV used in the photoionization scans, we must establish that m/z = 27 signal represents only the vinyl radical at this higher photoionization energy. Time profiles for m/z = 27 obtained at 10.214 and 10.814 eV are shown in Figure 2b; the fitted rise and decay constants are equivalent within 2σ uncertainty limits. This equivalence either means that the signal at 10.814 eV arises only from the vinyl radical, or that there is a daughter ion contributing to m/z = 27 at 10.814 eV that comes from a species with a time dependence nearly identical to that of the vinyl radical.

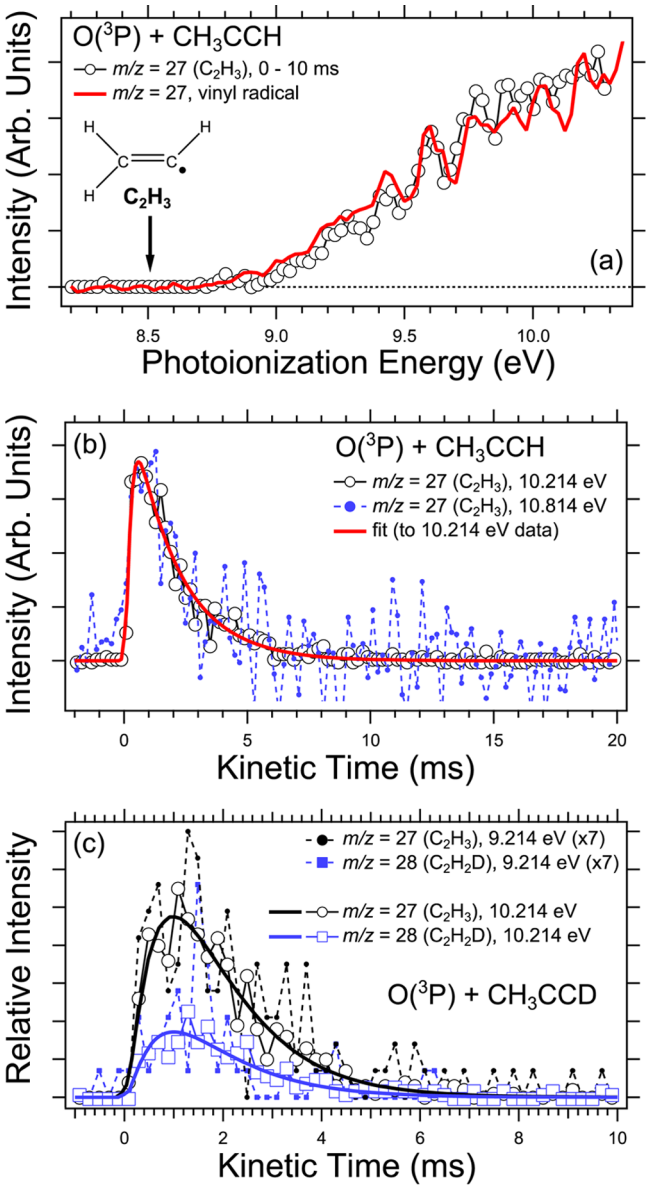

Figure 2. (a) Photoionization spectrum obtained for m/z = 27 (C_2H_3, from data between 0 and 10 ms after photolysis) generated by R1 (black circles) and a reference spectrum for the vinyl radical[44] (red trace). The black arrow marks the AIE of the vinyl radical reported in ref 45. (b) Time profiles for m/z = 27 from R1 obtained at 10.214 eV (open circles) and 10.814 eV (closed blue circles), arbitrarily scaled in intensity for comparison. A fit to the data at 10.214 eV is shown as a solid red line. (c) Time profiles for m/z = 27 (C_2H_3) and m/z = 28 (C_2H_2D) from $O(^3P)$ + d_1-propyne taken at 9.214 and 10.214 eV. Both traces obtained at 9.214 eV are scaled by a common factor for comparison with the 10.214 eV traces.

Only one observed time profile, at m/z = 55 (C_3H_3O, later shown to be predominantly methylketenyl), closely resembles the vinyl radical time profile. Therefore, we briefly consider the possibility that $C_2H_3^+$ daughter ions of methylketenyl contribute to the observed m/z = 27 signal. Below 10.3 eV, this possibility can be nearly ruled out because of the good agreement between m/z = 27 signal (present experiments) and the reference photoionization spectrum for the vinyl radical (Figure 2a). To determine whether at 10.814 eV we also probe only the vinyl radical at m/z = 27, we determined the branching ratio for the m/z = 27 signal relative to the (unrelated) NO side

DOI: 10.1021/acs.jpca.5b00491
J. Phys. Chem. A 2015, 119, 7388−7403

product from NO_2 photolysis (i.e., N_{vinyl}/N_{NO}) at both 10.214 and 10.814 eV using the vinyl radical photoionization cross-section to convert signal ratios to concentration ratios. The respective branching fractions from this approach, (0.12 ± 0.03) and (0.13 ± 0.05), are in excellent agreement, which would be unlikely if the m/z = 27 signal represents anything other than the vinyl radical. The ~30% uncertainty in these branching ratios likely reflects a conservative upper limit to the contribution of $C_2H_3^+$ produced by dissociative ionization of C_3H_3O. Although our determinations of the concentration of C_2H_3 are strictly upper limits to the true concentration (thus making other branching ratios lower limits to the true values), we see no strong evidence for contamination of m/z = 27 signal and conclude that m/z = 27 is due solely to the vinyl radical at both 10.214 and 10.814 eV, the photon energies we use to determine branching ratios.

In experiments employing d_1-propyne (CH_3CCD) at single photoionization energies between 9 and 10.3 eV, transient species relevant to R1a were observed at m/z = 27 (C_2H_3), 28 (C_2H_2D), 29 (HCO), and 30 (DCO, only partially resolved from strong NO signal). These observations are qualitatively consistent with the observation of both C_2H_3 + DCO and C_2H_2D + HCO product channels. Fits to kinetic traces obtained at 9.214 and 10.214 eV (see Figure 2c) indicate that the rise and decay of the C_2H_3 and C_2H_2D product signals are identical, and $N_{C_2H_3}/N_{C_2H_2D}$ = (2.8 ± 0.5). These values imply a slight difference from the results of Kanofsky et al.,[20] who reported $N_{C_2H_3}/N_{C_2H_2D}$ = (4.0 ± 1.0). The implications of these isotopologue yields will be discussed in section 4.

3.3. Channel R1b: CH_3 (m/z = 15) + HCCO (m/z = 41). Time-resolved signal for CH_3 at m/z = 15 was observed from R1, and the resulting kinetic trace at 10.214 eV and photoionization spectrum from data occurring up to 10 ms after photolysis are consistent with this signal belonging solely to the methyl radical (AIE = 9.84 eV, see Figure 3).[19,49,50] The AIE of the ketenyl radical (HCCO, m/z = 41) co-product of CH_3 from R1b is reported as 9.5 eV in the NIST web book,[51] whereas a recent calculation predicts AIE = 10.7 eV.[52] Our CBS-QB3 calculations for ionization of HCCO to the lowest-lying singlet state of the $HCCO^+$ yield an ionization energy of 10.8 eV, in good agreement with the previously calculated value. However, our calculations show that the ground electronic state of $HCCO^+$ is actually of triplet multiplicity, corresponding to AIE = 10.0 eV, in excellent agreement with the electron impact ionization threshold of (9.8 ± 0.3) eV reported in ref 52. As discussed at the beginning of section 3, we detect the HCCO radical in photoionization energy scans at photon energies below 10.3 eV, but the signal is partially obscured by overlap with signal from other species. In addition, absolute photoionization cross-section data are not available for HCCO. Thus, we find the methyl radical to be a more reliable indicator for R1b. Using the well-known absolute photoionization cross-section of the methyl radical with fits to the observed signal at 10.214 eV, we determine N_{methyl}/N_{vinyl} = N_{R1b}/N_{R1a} = (0.35 ± 0.11).[24,50,53,54]

In experiments employing d_1-propyne, the methyl radical was observed solely at m/z = 15 (i.e., only the d_0 isotopologue), implying that the methyl group on propyne leaves with no significant hydrogen scrambling. This result is in agreement with the observations of Kanofsky et al.,[20] who reported a negligible CHD_2 yield from R1 when using d_3-propyne, CD_3CCH. The DCCO co-product of CH_3 in the present d_1-propyne experiments could not be observed near m/z = 42 due to large background signal from ^{13}C d_1-propyne and a significant time-resolved d_0-ketene product signal.

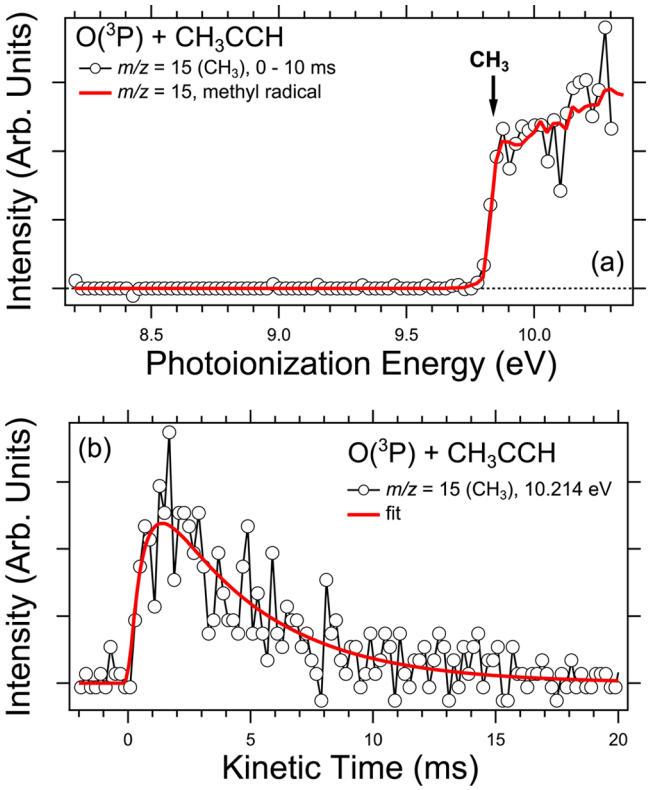

Figure 3. (a) Photoionization spectrum for the m/z = 15 (CH_3) product from R1 occurring between 0 and 10 ms after photolysis (black circles) and the known photoionization spectrum of the methyl radical (red trace).[24] The black arrow indicates the AIE of the methyl radical at 9.84 eV.[49] (b) Time profile for m/z = 15 obtained at 10.214 eV (black circles) and the accompanying fit (red trace).

3.4. Channel R1c: CH_3CCO (m/z = 55) + H (m/z = 1). A transient product was observed at m/z = 55 with sum formula C_3H_3O (Figure 4). The anticipated H-atom co-product of C_3H_3O produced via R1c was not detected in the present experiments due to a prohibitively high ionization energy (13.6 eV).[36] C_3H_3O was also identified as a major product in the CMB studies of Kanofsky et al.[20] and Balucani et al.[10] From observations of the various C_3H_3O isotopologues produced from reaction of $O(^3P)$ with CH_3CCD and CD_3CCH precursors, Kanofsky et al. concluded that H-loss from the acetylenic site (producing methylketenyl, CH_3CCO) is favored over H-loss from the methyl site by a factor of ~10.[20] Using laser-induced fluorescence to directly detect H- and D-atom formation from the $O(^3P)$ + CH_3CCD reaction at ~1 Torr and room temperature, Xing et al.[55] also found that ejection of the acetylenic H-atom was preferred, but only by a factor of 1.3.[55] Although there is no apparent cause for the discrepancy in the two experiments, it is possible that the measurements by Xing et al. were affected by H- and D-atoms produced by decomposition of other reaction products such as vibrationally excited HCO radicals. Unfortunately, minor contaminations in our d_1-propyne sample at m/z = 54 (and the associated ^{13}C isotopologue at m/z = 55) and m/z = 56 prevented observation of potential C_3H_3O (m/z = 55) and C_3H_2DO (m/z = 56) isotopologues in our $O(^3P)$ + CH_3CCD experiments.

DOI: 10.1021/acs.jpca.5b00491
J. Phys. Chem. A 2015, 119, 7388−7403

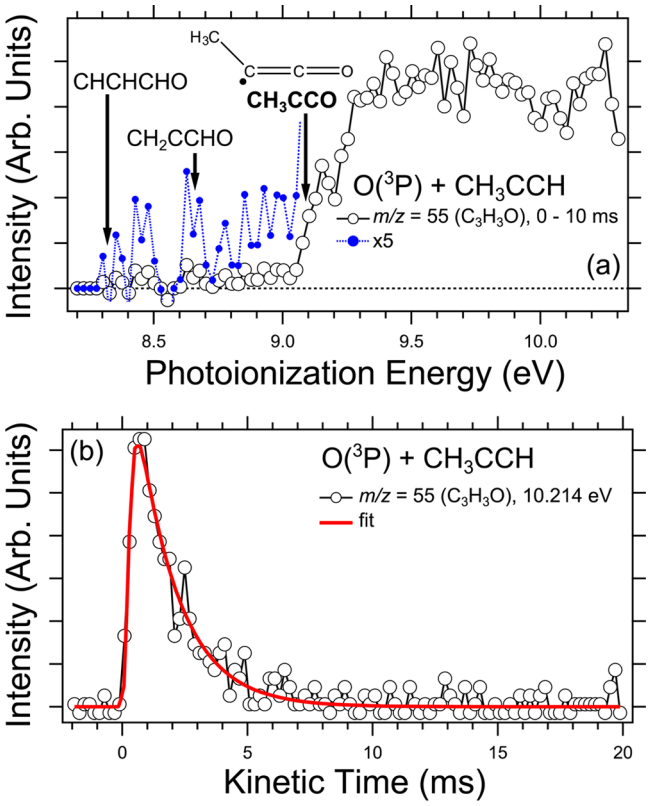

Figure 4. (a) Photoionization spectrum for m/z = 55 (C_3H_3O) from $O(^3P)$ + propyne between 0 and 10 ms after photolysis (open black circles). These same data magnified by a factor of 5 are shown by closed blue circles to illustrate minor signal below the AIE of the methylketenyl radical. AIEs for C_3H_3O isomers that are above 8.2 eV (see Table 2) are indicated by arrows. (b) Time profile for m/z = 55 from R1 obtained at 10.214 eV (black circles) and the accompanying fit (red trace).

The photoionization spectrum obtained for C_3H_3O (Figure 4a) from signal occurring between 0 and 10 ms after photolysis in the present d_0-propyne experiments indicates a sharp onset near 9.1 eV, although a much weaker contribution exists below this energy. In an investigation into the photodissociation dynamics of propenal (CH_2CHCHO), Chin et al. employed a variety of high-level computational methods to investigate the relative stability and AIEs of several C_3H_3O isomers (reported in Table 2).[56] It is clear that none of the AIE values reported by Chin et al. match the observed onset of signal at 9.1 eV in the present work. However, Chin et al. considered only transitions to singlet cation states and reported difficulties finding a minimum for the energetically lowest-lying singlet methylketenyl cation (CH_3CCO^+), as calculations instead converged to a CH_2CHCO^+ structure. Similar to HCCO (section 3.3), our CBS-QB3 calculations support that the ground electronic state of CH_3CCO^+ has triplet multiplicity and corresponds to AIE = 9.1 eV, in excellent agreement with the observed onset of signal in the C_3H_3O photoionization spectrum from R1. Weak signal below 9.1 eV may indicate the minor presence of isomers other than CH_3CCO, and likely corresponds to CH_2CCHO that can be formed by C−H bond cleavage after terminal addition of $O(^3P)$ to propyne.

Calculations by Zhao et al.[21] predicted that the formation of H + CH_3CCO from R1 is exothermic by −13 kcal/mol relative to reactants, and calculations by Chin et al.[56] suggested that H-atoms on CH_3CCO are bound by ∼47 kcal/mol, suggesting that H-loss from internally excited CH_3CCO produced via R1c is unimportant. Predominant formation of the methylketenyl isomer of C_3H_3O is in agreement with the observations of Kanofsky et al.[20] It furthermore supports that the larger H- vs D-atom ratio from $O(^3P)$ + d_1-propyne observed by Xing et al.[55] is contaminated by H-atom sources other than R1c.

Table 2. Adiabatic Ionization Energies and Relative Energies for Various C_3H_3O Isomers As Reported from Calculations in Ref 56 or CBS-QB3 Calculations Performed in the Present Work

C_3H_3O isomer	neutral state	relative energy (kcal/mol)[b]	cation state	AIE (eV)[b]
CH_3CCO	$^2A''$	0.0	$^1A'$[a]	9.57
			$^3A'$	9.09[c]
CH_2CHCO	$^2A''$	−10.3	$^1A'$	6.83
	$^2A'$	−10.9		6.86
CH_2CCHO	$^2A''$	8.1	$^1A'$	8.66
	$^2A'$	11.5		8.51
CHCHCHO	$^2A'$	11.1	^1A	8.32
			$^3A''$	10.34[c]
CHCCHOH	$^2A''$	11.8	$^1A'$	7.39
CH_2CCOH	$^2A''$	20.2	$^1A'$	7.50

[a]No minimum could be found; transition state for 1,2-H-atom transfer used instead. [b]As reported from CCSD(T) and B3LYP methods in ref 56, except where noted. [c]Determined using CBS-QB3 methods in the present work.

The absence of absolute photoionization cross-section data for CH_3CCO requires us to estimate its cross-section. Using semi-empirical methods,[57] we estimate a photoionization cross-section of (11.5 ± 5.8) Mb at an energy above the Franck−Condon envelope (assumed to be valid at 10.214 eV, cf. Figure 4a, see Supporting Information) resulting in the value $N_{methylketenyl}/N_{vinyl} = N_{R1c}/N_{R1a} = (0.18 \pm 0.10)$.[57] Our determination of $N_{methylketenyl}/N_{vinyl}$ is inversely proportional to the photoionization cross-section of methylketenyl and can be scaled accordingly if the cross-section is experimentally measured in future studies.

3.5. Channel R1d: C_2H_4 (m/z = 28) + CO (m/z = 28). We observed no signal at m/z = 28 (C_2H_4 or CO) corresponding to a product of R1d in the photoionization scans up to 10.313 eV, but we detected $C_2H_4^+$ signal in the single-energy experiments at 10.814 and 11.514 eV. Formation of the carbon monoxide (CO) co-product of C_2H_4 could not be investigated in the present study because of its prohibitively high AIE of 14.0 eV.[36] The large exothermicity for channel R1d means that both singlet ethene ($^1C_2H_4$) and excited triplet ethene ($^3C_2H_4$) accompanied by CO are potential products of R1d from the singlet and triplet C_3H_4O PESs, respectively (see Figure S2 in the Supporting Information). In addition, the energetic $^3CH_3CH$ ethylidene isomer of C_2H_4 has also been indicated as a potential product of R1.[20,55,58,59] The AIE for $^1C_2H_4$ of 10.51 eV[36] is certainly consistent with the photoionization energy dependence of the observed signal, but to our knowledge an AIE has not been reported for $^3CH_3CH$. The ground state of ethylidene[60] is $^3A''$ and CBS-QB3 calculations of this neutral species and the lowest-lying doublet cation ($^2A''$) indicate AIE = 7.40 eV. At 10.313 eV, the absence of signal at m/z = 28 or unidentified signal at lower m/z (i.e., from dissociative ionization) suggests that $^3CH_3CH$ is not formed via R1 or that it rapidly decomposes to form unknown products, or

DOI: 10.1021/acs.jpca.5b00491
J. Phys. Chem. A 2015, 119, 7388−7403

isomerizes prior to being ionized. The lowest-lying triplet state of ethene is ~2.7 eV above the singlet ground state,[21] and a lack of m/z = 28 signal at 10.313 eV also suggests that $^3C_2H_4$ is not directly observed. Thus, we conclude that the only C_2H_4 species we observe is ethene in its ground electronic state. Although we cannot definitely rule out formation of $^3C_2H_4$ or $^3CH_3CH$ followed by rapid deactivation/isomerization to $^1C_2H_4$, pathways leading to these products are disfavored based on calculated stationary points (discussed in section 4; see ref 21). However, there is evidence that at our experimental conditions (298 K and 4 Torr) vibrationally hot ethene formed by channel R1d decomposes to acetylene (C_2H_2) and other products, which will be discussed in more detail in section 4.1.

In the O(^{3}P) + CH_3CCD experiments, a stable product consistent with ethene was observed solely at m/z = 29 (C_2H_3D), albeit with some contributions from the HCO radical through 10 ms after photolysis.

Time traces for m/z = 28 produced via R1 in d_0-propyne experiments using photoionization energies of 10.814 and 11.514 eV are presented in Figure 5a and have identical rises within the experimental signal-to-noise. Using the absolute photoionization cross-section of ethene at 10.814 eV (Supporting Information), the observed ethene signal can be compared to the vinyl radical yielding $N_{ethene}/N_{vinyl} = N_{R1d}/N_{R1a}$ = (0.73 ± 0.27) at 4 Torr and 298 K.

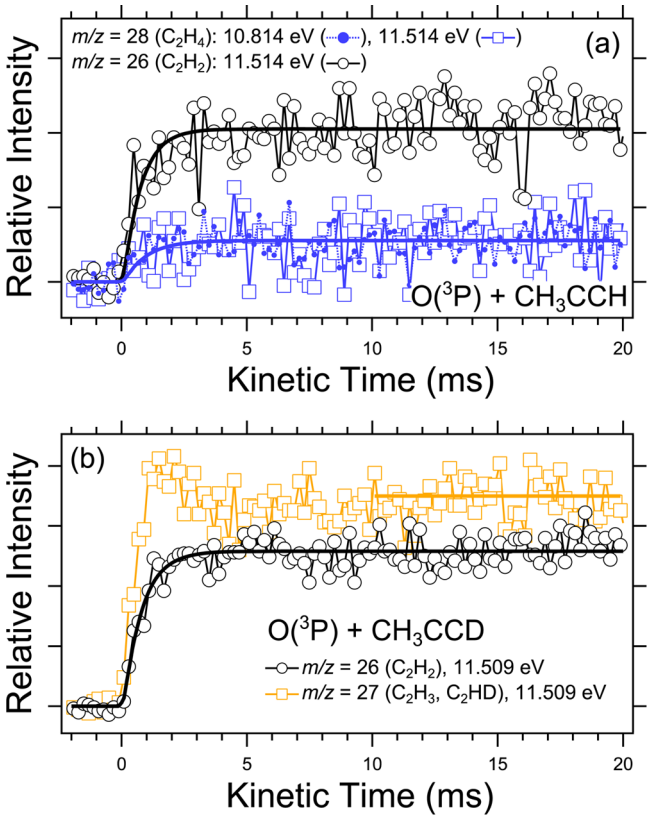

Figure 5. (a) Time profiles for m/z = 28 (C_2H_4) obtained at photoionization energies of 10.814 eV (solid blue circles) and 11.514 eV (open blue squares) and m/z = 26 (C_2H_2) obtained at 11.514 eV (open black circles) from R1. Fits to the 11.514 eV data are also shown. The relative intensity of the two time profiles obtained at 11.514 eV is retained, although the 10.814 eV m/z = 28 signal is scaled for comparison with signal at 11.514 eV. (b) Time profiles for m/z = 26 (C_2H_2) and m/z = 27 (C_2H_3 and C_2HD) obtained at 11.509 eV from O(^{3}P) + CH_3CCD experiments along with the accompanying fits.

3.6. Channel R1e: C_2H_2 (m/z = 26) + H_2 (m/z = 2) + CO (m/z = 28). A C_2H_2 product from R1 was observed in single energy experiments with an appearance energy between 10.814 and 11.514 eV, consistent with formation of acetylene (AIE = 11.40 eV).[36] The co-products of direct channels of R1 forming acetylene include H_2CO and H_2 + CO, none of which could be observed in the present experiments for reasons previously mentioned. Thus, from the experimental data we cannot directly discern if the co-product(s) of acetylene is H_2CO (channel R1e′), H_2 + CO (channel R1e), or some combination of both, although we later argue that the concerted three-body C_2H_2 + H_2 + CO channel R1e dominates. As discussed later (section 4.1), acetylene may also be produced via decomposition of chemically activated ethene from R1d.

At 11.514 eV, signal for the vinyl radical at m/z = 27 for direct determination of $N_{acetylene}/N_{vinyl}$ from R1 is barely resolvable from background signal. However, ethene is still observable at this photon energy. In order to evaluate $N_{acetylene}/N_{vinyl}$, we use the product of $N_{acetylene}/N_{ethene}$ measured at 11.514 eV and N_{ethene}/N_{vinyl} at 10.814 eV (derived in the previous section). Using the photoionization cross-section for acetylene at 11.514 eV (see Supporting Information) and the extracted signal from a fit of the time traces for acetylene and ethene allows determination of $N_{acetylene}/N_{ethene}$ = (1.80 ± 0.53), in excellent agreement with the value of ~2 determined from gas chromatography investigations of R1 near 298 K and 4 Torr.[58] Using the product of our value of $N_{acetylene}/N_{ethene}$ and N_{ethene}/N_{vinyl} from the previous section yields $N_{acetylene}/N_{vinyl} = N_{R1e}/N_{R1a}$ = (1.31 ± 0.62) under our experimental conditions.

In O(^{3}P) + CH_3CCD experiments at 11.509 eV, time-resolved signal consistent with acetylene was observed at both m/z = 26 (C_2H_2) and 27 (C_2HD) as shown in Figure 5b. Signal for a stable HDCO isotopologue of formaldehyde (m/z = 31, a potential co-product of C_2H_2) was observed at 11.509 eV, whereas the potential H_2CO co-product of C_2HD at m/z = 30 was not observable due to large background signal from NO. A fit to the observed HDCO time profile at m/z = 31 yields a formation rate of (390 ± 70) s^{-1}, suggesting that the majority of the observed d_1-formaldehyde product results from secondary chemistry.

At early kinetic time (0–10 ms after photolysis) the m/z = 27 trace obtained for C_2HD at 11.509 eV in d_1-propyne experiments also contains contributions from d_0-vinyl (see Figure 5b). By 10 ms after photolysis the combined kinetic profile for both m/z = 27 species is stable and should arise solely from d_1-acetylene. Comparison of the mean signal between 10 and 20 ms after photolysis for both the m/z = 26 and 27 traces obtained at 11.509 eV results in a branching ratio $N_{C_2H_2}/N_{C_2HD}$ = (0.80 ± 0.004). Xing et al.[55] reported the observation of both H_2 and HD from the reaction of O(^{3}P) with d_1-propyne with a branching ratio of N_{HD}/N_{H_2} = (0.71 ± 0.15), in excellent agreement with the ratio $N_{C_2H_2}/N_{C_2HD}$ observed here and, importantly, supporting a correlation between production of H_2 and acetylene.

3.7. Channel R1f: C_3H_3 (m/z = 39) + OH (m/z = 17). Weak signal was observed at m/z = 39 consistent with the sum formula C_3H_3. A minor m/z = 39 species was also observed in the CMB experiments by Kanofsky et al.,[20] although evidence for R1f was not reported in the ~9 kcal/mol collision energy CMB experiments by Baluncani et al.[10] In the present

DOI: 10.1021/acs.jpca.5b00491
J. Phys. Chem. A 2015, 119, 7388–7403

experiments, a significant background signal at $C_3H_3^+$ from dissociative ionization of propyne, ionized by higher harmonic radiation escaping the rare gas filter of the synchrotron light source, made it difficult to obtain a usable signal-to-noise ratio for identification via photoionization scans. Transient C_3H_3 signal was observed in single energy experiments as low as 9.009 eV, consistent with assignment as the propargyl radical (CH_2CCH, AIE = 8.70 eV).[61] Formation of OH + propargyl from R1 is exothermic with respect to reactants by −4.4 kcal/mol;[21] other C_3H_3 isomers lie >40 kcal/mol above the ground state of propargyl and are not accessible under the present conditions.[62] In experiments employing d_1-propyne, evidence for propargyl appeared solely at m/z = 40 (C_3H_2D), suggesting that propargyl is formed by H-abstraction from the methyl group on propyne. Formation of the hydroxyl radical (OH, m/z = 17) co-product of the propargyl radical from channel R1f was not observable, again due to a prohibitively high AIE (13.0 eV).[36]

Unfortunately, the signal-to-noise in the observed m/z = 39 data prevents assignment of this product to formation via primary or secondary chemistry. Using signal determinations at 10.214 eV and the known absolute photoionization cross-section of the propargyl radical,[24,63] we determine $N_{propargyl}/N_{vinyl}$ = (0.04 ± 0.02). As discussed later, a minor yield of R1f is certainly reasonable, although we cannot rule out that the observed propargyl product results from secondary chemistry.

3.8. Channel R1h: CH_2CCO (m/z = 54) + H_2 (m/z = 2). In d_0-propyne experiments, a stable product was observed at m/z = 54 with a sum formula of C_3H_2O, although the signal was very weak (<5% of the signal intensity for the vinyl radical at 10.214 eV). A minor C_3H_2O product from R1 was previously observed in CMB studies by Balucani et al.[10] H_2, the anticipated co-product of C_3H_2O, has also been previously observed.[55] However, in the same way that there are many pathways in R1 that can form CO, there are also multiple H_2-generating pathways, making observation of C_3H_2O a more definitive candidate for characterization of R1h. Calculations by Zhao et al.[21] and Chin et al.[22] suggested that both the propadienal (CH_2CCO) and 2-propynal (CHCCHO) isomers of C_3H_2O are thermodynamically allowed products of R1h, with propadienal being energetically favored.

A photoionization spectrum for the observed C_3H_2O product is shown in Figure 6. CBS-QB3 calculated AIEs for propadienal and 2-propynal are 9.13 and 10.74 eV, respectively, in close agreement with previous experimental determinations.[64−68] The calculated AIE for propadienal is indicated by a black arrow in Figure 6, and coincides with the observed onset of signal in the spectrum supporting minor formation of propadienal. However, the limitation of photoionization scans to energies less than 10.3 eV in the present measurements means we can neither confirm nor exclude production of 2-propynal from R1h. At 10.814 eV signal at m/z = 54 cannot be distinguished from background signal, and if 2-propynal is produced it would have a minor signal and overall yield.

Low signal-to-noise prevents the conclusive assignment of C_3H_2O as a direct product of R1, although its minor signal is qualitatively consistent with the CMB measurements by Balucani et al.[10] Furthermore, as discussed in section 3.4, contaminants in the d_1-propyne sample prevented detection of m/z = 54 (C_3H_2O) and m/z = 55 (C_3HDO) in those experiments. In the absence of an absolute photoionization spectrum for propadienal, we estimated an absolute photoionization cross-section of (29 ± 14.5) Mb at 10.214 eV,[57]

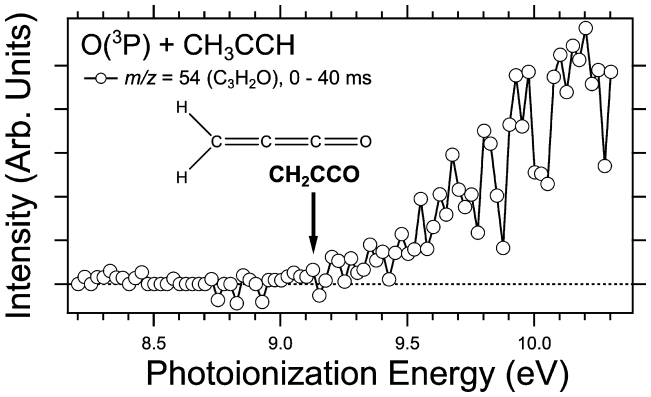

Figure 6. Photoionization spectrum for the stable m/z = 54 (C_3H_2O) product obtained from the reaction of O(^{3}P) with propyne from data between 0 and 40 ms after photolysis. The CBS-QB3 calculated AIE of propadienal (CH_2CCO) is indicated by the arrow at 9.13 eV. The 2-propynal isomer (CHCCHO) has a calculated AIE of 10.74 eV and would not be detected in the photoionization scans performed here up to 10.3 eV.

which suggests the almost negligible branching ratio $N_{propadienal}/N_{vinyl}$ = (0.005 ± 0.002) under our experimental conditions.

4. DISCUSSION

We assign signals for vinyl, methyl, methylketenyl, ethene, and acetylene to primary products of R1 from channels R1a, R1b, R1c, R1d, and R1e, respectively. We also observe minor production of the propargyl radical and propadienal, although we cannot definitively assign these as direct products of R1f and R1h. The ketene (C_2H_2O) product observed in the present experiments is assigned as a secondary product based on its time profile (see Supporting Information). The branching ratios for the observed channels are summarized in Table 1. Under the assumption that we account for all of the direct products of R1, these branching ratios can be converted to branching fractions at 4 Torr and 298 K, which are also given in Table 1. Based on these results, R1a (C_2H_3 + HCO), R1d (C_2H_4 + CO), and R1e (C_2H_2 + H_2 + CO) are the major channels of R1, accounting for a total of (84 ± 14)% of the products of R1.

In the following sections, these isomer-resolved branching fractions and the observed isotopologue yields from d_1-propyne experiments will be used to discuss active mechanisms in R1 at 4 Torr and 298 K.

4.1. Decomposition and Energetic Forms of C_2H_4. The nature of the C_2H_4 product from R1 has been a topic of considerable debate. However, a majority of the discussion stems from experimental observation of internal energy distributions in the CO product of R1, and the present results identify significant yields of multiple CO-forming product channels (R1d, R1e, and possibly decomposition of hot HCO formed via R1a) making it likely that CO carries convoluted dynamical information from multiple mechanistic pathways.[21,55,58,59] Calculations by Zhao et al.[21] showed that pathways leading to energetic forms of C_2H_4, such as triplet ethene ($^3C_2H_4$) and triplet ethylidene ($^3CH_3CH$), are characterized by high-lying barriers and are unlikely to be competitive at low temperature. Many of these calculated stationary points are presented in Figure 7. Coupled with the observation of ethene only in its ground electronic state in the present work, we assume that the only significant channel

DOI: 10.1021/acs.jpca.5b00491
J. Phys. Chem. A 2015, 119, 7388−7403

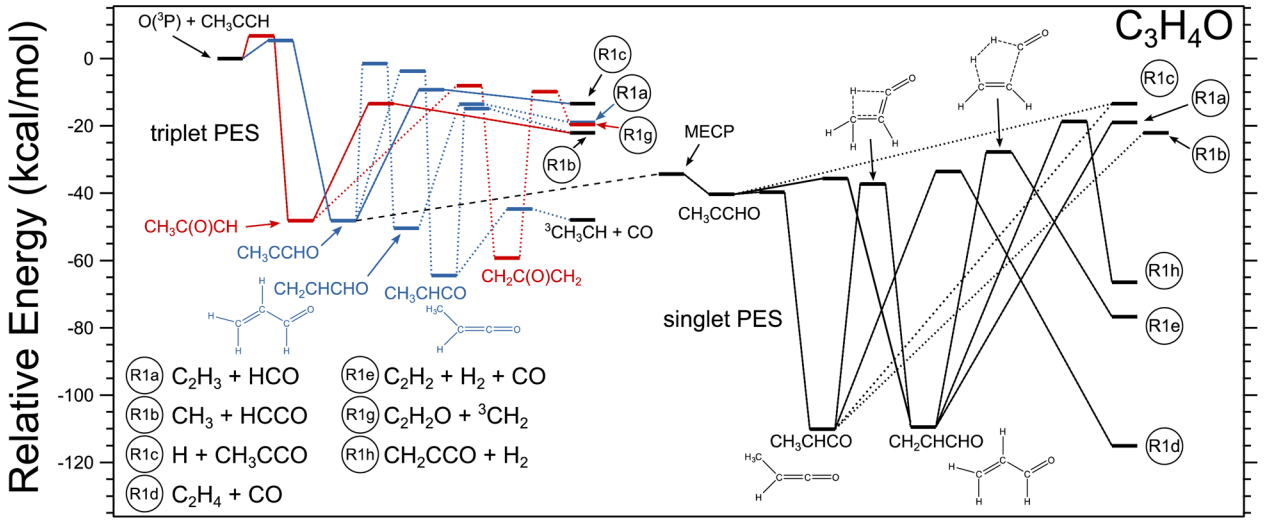

Figure 7. Relevant stationary points on the C_3H_4O potential energy surfaces for the reaction of $O(^3P)$ + propyne taken from CCSD(T)/6-311G(d,p)//B3LYP/6-311G(d,p) calculations in ref 21. The triplet PES accessed by addition of $O(^3P)$ to the central carbon atom in propyne (i.e., C_2) is indicated by red and that accessed by addition to the terminal carbon atom (i.e., C_1) is indicated by blue. The singlet C_3H_4O PES is represented by black. Saddle points separating R1b from C_3H_4O isomers on the singlet PES were not reported in ref 21 and would be of interest in future investigations of this PES. Pathways believed to be active at 4 Torr and 298 K are indicated by solid lines.

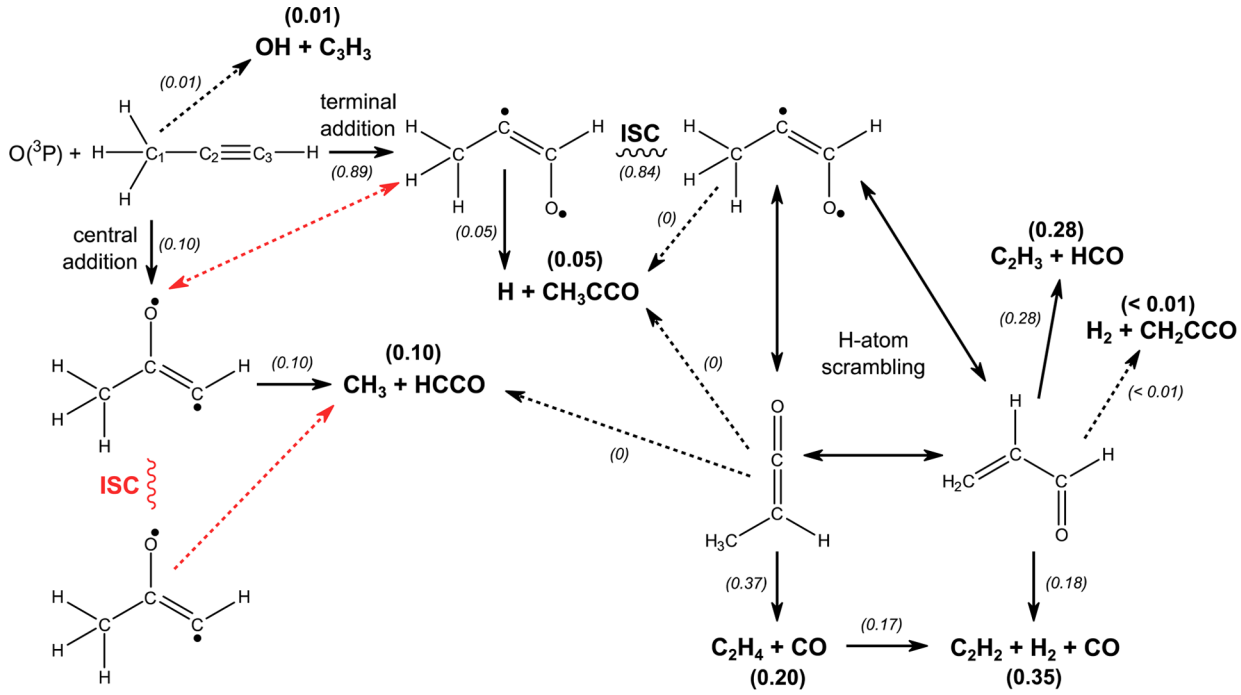

Figure 8. Active mechanisms leading to bimolecular products based on the present observations of R1 at 298 K and 4 Torr. Solid and dashed arrows represent major (>5% of total yield) and minor pathways, respectively, and the measured branching fractions for the various product channels are indicated in bold (see also Table 1). Pathways in red have not been characterized computationally and would be of considerable interest in future studies. Limiting our analysis to the pathways characterized in ref 21, estimated fluxes through each step of the $O(^3P)$ + propyne reaction are shown as italicized text near arrows (see text for more details).

forming C_2H_4 is R1d, in which both C_2H_4 and CO are formed in their ground electronic states. However, R1d is highly exothermic (ΔH_{rxn} = −115.1 kcal/mol), and it is possible that ethene is formed with enough internal energy to undergo subsequent dissociation to other products on a time scale that is fast compared to the present measurements.

In gas chromatography experiments, Lin et al.[58] observed a strong pressure dependence for $N_{acetylene}/N_{ethene}$ at 298 K, which decreases from a value of ∼2.6 at 2 Torr, to ∼2 near our 4 Torr conditions (versus ∼1.8 determined here), to ∼0.5 near 600 Torr. These results are consistent with two competing pathways for C_2H_2 formation: a concerted mechanism forming C_2H_2 + H_2 + CO (R1e), and formation of a vibrationally excited C_2H_4 molecule that can either decompose to C_2H_2 + H_2 or be collisionally stabilized. (Decomposition to C_2H_3 + H is very unlikely at room temperature, see Supporting Information.) Our reported branching fractions are the observed yields of the various product channels at 4 Torr

DOI: 10.1021/acs.jpca.5b00491
J. Phys. Chem. A 2015, 119, 7388−7403

and 298 K. However, the flux through these two pathways that produce acetylene is better determined at high pressure, where collisional deactivation of vibrationally excited C_2H_4 from R1d dominates over its decomposition to C_2H_2 + H_2. Using the total yield of R1d (20% of the observed products of R1) and R1e (36% of the observed products) determined in the present work (i.e., a combined yield of 56%) and the observation by Lin et al. that $N_{acetylene}/N_{ethene} \approx 0.5$ at 600 Torr (the highest pressure for which data are available in that study), we estimate that 37% of the reactive flux of R1 leads to R1d and 19% leads to R1e. At 4 Torr and 298 K, almost half of the C_2H_4 produced by R1d undergoes dissociation to C_2H_2 + H_2. Single collision CMB experiments would provide yields in the zero-pressure limit, where R1e should have a larger yield at the expense of R1d. Comparisons between the reactive flux through pathways of R1 and our measured branching ratios at 4 Torr and 298 K are shown in Figure 8.

4.2. Triplet Potential Energy Surface. Zhao et al.[21] reported stationary points on the lowest-lying triplet and singlet C_3H_4O PESs in regions relevant to R1. Stationary points relevant to observations in our experiments are presented in Figure 7 to aid the ensuing discussion. R1 may begin with either addition of $O(^3P)$ to one of the unsaturated carbon atoms of propyne (i.e., C_1 or C_2) or by abstraction of a H-atom. The calculated barrier to H-atom abstraction to form C_3H_3 + OH (R1f) is 11.7 kcal/mol above the 0 K reactants energy. This pathway accounts for ∼1% of the observed products in the present work and was not reported in the CMB experiments at ∼9 kcal/mol collision energy by Balucani et al.[10] Because propargyl could not definitively be assigned as a direct product from R1 in the present work, the yield from R1 under our conditions may be even lower than 1%. By comparison, we did not observe any evidence for H-atom abstraction in the case of $O(^3P)$ + propene at 298 K and 4 Torr,[19] where the associated barriers are >15 kcal/mol above the reactants.[69]

The remaining products of R1 are formed via addition of $O(^3P)$ to propyne, which occurs with significantly lower barriers (∼6 kcal/mol above reactants) when compared to H-abstraction. Addition to the central (i.e., C_2) carbon atom of propyne results in a resonance stabilized $CH_3C(O)CH$ triplet biradical that is stable with respect to reactants by 48.2 kcal/mol. This triplet adduct may dissociate to form CH_3 + HCCO (R1b) after traversing a barrier at −13.4 kcal/mol relative to reactants, which, for reasons discussed below, is the most likely route to R1b (10% of observed products). Triplet $CH_3C(O)CH$ may also isomerize by 1,3-H-atom shift via a barrier at −8.1 kcal/mol to form triplet $CH_2C(O)CH_2$, the most likely initial adduct from $O(^3P)$ + allene, which can subsequently dissociate to form ketene and $^3CH_2$ (R1g) over a barrier at −9.8 kcal/mol. This isomerization/dissociation is both energetically and entropically disfavored compared to R1b, in line with the fact that in the present experiments ketene is predominantly from secondary chemistry (although we cannot exclude minor amounts from R1g).

The calculated barrier for terminal addition of $O(^3P)$ to propyne (i.e., to C_1) to form the resonance stabilized triplet biradical CH_3CCHO is 1.3 kcal/mol lower than that for central addition, although the corresponding triplet C_3H_4O adducts are nearly isoenergetic. The lower barrier for terminal addition (5.4 kcal/mol relative to reactants) supports the general assertions of Cvetanovic that $O(^3P)$ will preferentially add to the least-substituted unsaturated carbon atom.[2] The energetically lowest-lying pathway from CH_3CCHO on the triplet surface is loss of the H-atom from the C_1 carbon atom to form a methylketenyl co-product (R1c, barrier at −9.3 kcal/mol relative to reactants), which was observed in the present experiments. Again based on arguments presented below, this triplet pathway is the most likely route to R1c (5% yield). The barrier for loss of a methyl H-atom to form CH_2CCHO is 8.2 kcal/mol higher in energy and should therefore be disfavored, corroborated by only minor signal that can possibly be attributed to CH_2CCHO in the present work.

Like the central adduct, isomerization of the CH_3CCHO terminal adduct is unlikely to compete with the bond fission reaction R1c at 298 K. Interestingly, the only identified route to form $^3CH_3CH$ + CO is via such an isomerization, and the computational results from Zhao et al.[21] do not support this channel as viable.

To summarize, the most likely bimolecular channels occurring on the triplet PES are production of CH_3 + HCCO (R1b) directly from the central adduct from R1 and production of H + CH_3CCO (R1c) directly from the terminal adduct. Our analysis finds a branching ratio of N_{R1b}/N_{R1c} = (1.9 ± 1.3). Although the uncertainty is quite large in our determination of N_{R1b}/N_{R1c}, it appears that our value is in only moderate agreement with N_{R1b}/N_{R1c} = (3.1 ± 0.6) reported by Balucani et al.[10] The reason for this discrepancy is not clear; the two branching ratios were determined at different conditions (298 K versus ∼9 kcal/mol collision energy) and in both measurements the methylketenyl yield is based on an estimated ionization cross-section. Future experiments characterizing the absolute photoionization and electron impact ionization cross-sections of methylketenyl would be of considerable interest.

All other observed channels are difficult to rationalize on the triplet C_3H_4O PES and likely result after ISC to the singlet C_3H_4O PES (see the following section). Ultimately the overall yield of R1b + R1c, which marks an upper limit to product formation on the triplet C_3H_4O PES, is small (∼15%), suggesting facile ISC in R1.

4.3. Intersystem Crossing and the Singlet Potential Energy Surface. A minimum energy crossing point (MECP) between the lowest-lying singlet and triplet C_3H_4O PESs was found by Zhao et al.[21] near the geometry of the terminal $O(^3P)$ + propyne adduct (CH_3CCHO) at 34.3 kcal/mol below the reactant energy (Figure 7). It is unlikely that the initial triplet CH_3CCHO and $CH_3C(O)CH$ adducts can interconvert (we calculate a CBS-QB3 energy of −1.2 kcal/mol relative to reactants for the transition state (TS) separating the two triplet adducts, too large to compete with the bond fission reactions) and therefore the two adducts likely mark two unique entry points on the triplet C_3H_4O PES. Balucani et al.[10] observed a 3.1:1 preference of R1b (CH_3 + HCCO) arising from the central adduct over R1c (H + CH_3CCO) arising from the terminal adduct. From these observations, the authors concluded that ISC does not significantly compete with dissociation in the region of the central adduct. However, because a localized singlet/triplet crossing point near the central addition adduct has not been described, nor has the related region of the singlet C_3H_4O PES been investigated, future studies exploring the role of ISC in this locale would be of interest. In addition, it is possible that excited singlet and triplet states can play a role in the reactions of $O(^3P)$ with linear unsaturated hydrocarbons[14,70] and exploring coupling seams involving these PESs would also be of interest.

DOI: 10.1021/acs.jpca.5b00491
J. Phys. Chem. A 2015, 119, 7388−7403

Although there are likely to be several points at which ISC occurs following terminal addition of $O(^3P)$ to propyne, the MECP located by Zhao et al.[21] is significantly lower in energy than barriers to isomerization and dissociation on the triplet C_3H_4O PES and, depending on the spin−orbit coupling strength, may suggest facile ISC at this locale. Unlike the case of $O(^3P)$ + propene,[71] a minimum has been identified on the singlet C_3H_4O PES (6 kcal/mol below the MECP and 40.3 kcal/mol below the reactant energy) at a geometry similar to that of the initial triplet CH_3CCHO adduct. It is possible that this deeper minimum resulting from resonance stabilization of the adduct plays a role in enhancing the rate of ISC in $O(^3P)$ + propyne when compared to $O(^3P)$ + propene (where ISC was estimated to account for ∼40% of the reaction products).[19]

Assuming the singlet PES is accessed solely via ISC near the geometry of the CH_3CCHO terminal adduct (due to the absence of calculated crossing points near the central adduct), this species can potentially dissociate on the singlet PES to H + CH_3CCO (R1c, −13.4 kcal/mol relative to reactants). Although associated with tighter TSs, pathways leading to isomerization of singlet CH_3CCHO lie so much lower in energy than the pathway to H + CH_3CCO that the latter appears to be unlikely. In addition, because CH_3CCO is resonance stabilized, there may be a small barrier separating it from CH_3CCHO, further disfavoring R1c (and also R1b) on the singlet PES. By contrast, isomerization of singlet CH_3CCHO via 1,2-H-atom shifts can occur to form methylketene (CH_3CHCO) or propenal (CH_2CHCHO) over relatively low barriers (−39.7 and −35.7 kcal/mol relative to the reactants, respectively).

If we accept that the main fate of the CH_3CCHO adduct on the singlet surface will be isomerization to methylketene and propenal, then the branching from these two wells to bimolecular products will be determined by a competition between tighter TSs at lower energies and looser TSs at higher energies. As shown in Figure 7, the tighter TSs control methylketene ↔ propenal isomerization and formation of singlet + singlet bimolecular products R1d, R1e, and R1h, whereas the looser TSs lead to the doublet + doublet channels R1a, R1b, and R1c.

On the triplet surface, none of the pathways are loose, barrierless processes, with R1b and R1c clearly being the most favored channels. Therefore, the most likely path to R1a (C_2H_3 + HCO), which has a larger experimental branching fraction than R1b and R1c combined, will not be on the triplet surface, but on the singlet surface via a barrierless pathway from propenal. Production of R1a on the singlet surface is also supported by isotopologue yields from d_1-propyne experiments discussed in the following section. The TS leading from propenal to C_2H_2 + H_2 + CO (R1e) lies lower in energy than R1a and could move propenal population toward R1e, although this TS is likely to be tighter than that leading to R1a. The fact that R1a is a significant product channel means that its higher entropy/higher energy TS can compete effectively with the lower entropy/lower energy TS leading to C_2H_2 + H_2 + CO (R1e). Propenal can also lead to C_2H_2 + H_2CO products (R1e′), although the TS leading to this channel (not shown in Figure 7) lies ∼12 kcal/mol higher in energy than that leading to C_2H_2 + H_2 + CO.[22] The energetically lower-lying concerted three-body C_2H_2 + H_2 + CO product channel (R1e) has been shown to be overwhelmingly favored in 193 nm (148 kcal/mol) photodissociation of propenal.[22,72,73] Although those experiments probe the C_3H_4O PES ∼40 kcal/mol above the energy available here, we assume that C_2H_2 + H_2 + CO (R1e) is dominant over C_2H_2 + H_2CO (R1e′) and accounts for ∼19% of the reactive flux.

From the methylketene well on the singlet C_3H_4O surface, the lower energy but tighter TSs control isomerization to propenal and formation of C_2H_4 + CO (R1d), whereas a higher energy but looser TS leads to CH_3 + HCCO (R1b). Experimentally, the large yield of R1d (accounting for 20% of the observed products at 4 Torr and potentially 37% of the reactive flux) implies that the low energy but tight TS from methylketene to R1d dominates compared to the higher energy pathway to R1b. A full master equation treatment including triplet-singlet coupling is beyond the scope of this paper, but these experimental measurements provide some insight into the competition between energy and entropy in the dynamics of the singlet surface, and are consistent with the nature of the calculated stationary points. Production of R1b and R1c on the singlet PES are also disfavored based on the observed isotopologue yields from d_1-propyne experiments discussed in section 4.4.

4.4. Isotopologue Yields from $O(^3P)$ + CH_3CCD. The experimental branching ratios together with the stationary points of Figure 7 help limit the potential mechanistic pathways giving rise to the observed products of R1. However, multiple routes to some product channels are possible and the observation of isotopologue yields in products of $O(^3P)$ + CH_3CCD helps to further constrain the active mechanisms. In the present experiments, we observe significant d_0- and d_1-vinyl radical yields from R1a ($N_{C_2H_3}/N_{C_2H_2D}$ = (2.8 ± 0.5)) and d_0- and d_1-acetylene yields from R1e ($N_{C_2H_2}/N_{C_2HD}$ = (0.80 ± 0.004)), but we do not observe d_1-methyl radicals resulting from R1b. Experimental interferences prevented us from observing the isotopologue distribution of the CH_3CCO product from R1c, although previous CMB experiments[20] identified almost exclusive production of the d_0 isotopologue. Likewise, we were unable to observe the isotopologue yield in the CH_2CCO + H_2 (R1h) channel.

On the singlet C_3H_4O (C_3H_3DO) PES, acetylene may be produced directly via R1e (through singlet propenal) or indirectly by decomposition of excited C_2H_4 generated from R1d (requiring passage through a methylketene intermediate). Based on stationary point structures and energies reported in refs 21 and 22 (see Supporting Information), only d_0-acetylene is expected to be formed through the propenal pathway CH_3CCDO → CH_2CHCDO → R1e on the singlet C_3H_4O PES. Decomposition of hot d_1-ethene produced via R1d could be a potential source of d_1-acetylene, although such a large yield of d_1-acetylene is hard to reconcile with this as the sole source of its production.

Our observation of a sizable yield of d_1-vinyl radical ($N_{C_2H_3}/N_{C_2H_2D}$ = (2.44 ± 0.56)) is also difficult to explain using a straight path from the MECP to products. The only plausible pathway to C_2H_3 + HCO (R1a) on the singlet C_3H_4O PES is via fission of the $CH_2CH-CHO$ bond in a propenal intermediate. From a direct CH_3CCDO → CH_2CHCDO → R1a path we would expect only formation of d_0-vinyl. However, a pathway involving isomerization of the singlet terminal adduct to methylketene and then propenal prior to dissociation to R1a (e.g., CH_3CCDO → CH_3CDCO → CH_2CDCHO → R1a) could explain the presence of d_1-vinyl. This pathway would also provide a source of d_1-acetylene if the d_1-propenal intermediate in this scheme (CH_2CDCHO) decomposes via R1e. The

DOI: 10.1021/acs.jpca.5b00491
J. Phys. Chem. A 2015, 119, 7388−7403

relatively low barrier heights for isomerization may induce facile H-atom scrambling via competing isomerization of the CH_3CCDO entry point on the singlet PES to methylketene and propenal, and subsequent methylketene ↔ propenal isomerizations (see Figure S3 in the Supporting Information). Because exit channels on the singlet PES lie higher in energy than this isomerization barrier, several iterations of the scrambling process may be possible.[74]

Prohibitively high barriers for isomerization of the triplet adducts to form methylketene or propenal (compared to other lower barriers on the singlet surface) suggest that this H-atom scrambling process is unique to the singlet PES. The products of R1b (CH_3 + HCCO) and R1c (H + CH_3CCO) do not show evidence for H-atom scrambling, supporting our assignment that they occur from the triplet central and terminal addition adducts, respectively. In further support of this assignment, Balucani et al.[10] observed CH_3 and CH_3CCO translational energy distributions that peak away from zero in their CMB experiments on R1, evidence for a significant barrier to formation of R1b and R1c which can only occur on the triplet C_3H_4O PES. It should be again noted that the singlet PES in the region of the central addition adduct has not been characterized, and some of the flux through R1b, likely minor, could potentially arise after ISC.

In light of the present analysis, we conclude that formation of CH_3 + HCCO (R1b), H + CH_3CCO (R1c), and C_3H_3 + OH (R1f) are likely to occur predominantly on the triplet C_3H_4O PES whereas C_2H_3 + HCO (R1a), C_2H_4 + CO (R1d), C_2H_2 + CO + H_2 (R1e), and CH_2CCO + H_2 (R1h) occur solely on the corresponding singlet PES. Figure 8 presents these assignments in black, with pathways warranting further investigation marked in red. In addition, because the only reasonable decomposition pathway from the central addition adduct $CH_3C(O)CH$ is formation of CH_3 + HCCO (R1b), and because this channel is unlikely to be formed on the singlet surface, we can also determine the site selectivity of addition from our data. Using these assignments, we estimate that at 298 K and 4 Torr less than 1% of R1 proceeds by H-abstraction, 10% of the observed products come from addition of $O(^3P)$ to the central carbon atom in propyne, and 89% come from terminal carbon atom addition.

4.5. Extent of Intersystem Crossing. Using our assignment of the active mechanisms in R1 and the branching fractions determined here, we find that (84 ± 14) % of the total reaction must proceed as a result of ISC. This value is a lower limit that assumes all of R1b and R1c occurs via the triplet PES. The extent of ISC observed for $O(^3P)$ + propyne is slightly lower than the result from CMB experiments on the $O(^3P)$ + allene reaction, which suggest that >90% of products result from ISC on the underlying C_3H_4O PES,[9] but significantly larger than the value of ∼40% determined for the reaction of $O(^3P)$ with the more saturated three-carbon propene molecule.[19] Recalling that in the $O(^3P)$ + acetylene reaction there is no experimental evidence for ISC, it is interesting that simple methyl substitution in acetylene causes a significant increase in the importance of ISC. The C_2H_2O adduct has only 9 vibrational degrees of freedom, whereas the C_3H_4O adduct has 18 vibrations. If the probability for ISC is low in both systems, the higher density of states in C_3H_4O should enable longer intermediate lifetimes, allowing many more attempts for the low-probability event of ISC to succeed. It is interesting to consider why, among all the linear unsaturated C_2 and C_3 hydrocarbons, all but acetylene fall in the range of 30−90% ISC despite such dramatic differences in adduct exothermicity, and presumably also variation in the energy of the MECP. In this regard, future work on $O(^3P)$ reactions with C_4 hydrocarbons would be of great interest.

5. CONCLUSIONS

The present work provides the first comprehensive quantitative and isomer-resolved account of the products of the $O(^3P)$ + propyne reaction at 4 Torr and 298 K. We find five major product channels: C_2H_3 + HCO, CH_3 + HCCO, H + CH_3CCO, C_2H_4 + CO, and C_2H_2 + H_2 + CO. Aided by quantum chemical calculations[21] and experiments employing isotopically substituted propyne, we conclude that the CH_3 + HCCO and H + CH_3CCO channels occur on the initial triplet PES accessed by the $O(^3P)$ + propyne reaction, and that the C_2H_3 + HCO, C_2H_4 + CO, and C_2H_2 + H_2 + CO channels occur after ISC to the singlet PES. Contributions from C_3H_3 + OH and CH_2CCO + H_2 product channels (from the triplet and singlet PESs, respectively) are too small to conclusively assign them as direct channels from $O(^3P)$ + propyne. Branching fractions and active mechanisms determined here suggest that (84 ± 14)% of the total product yield occurs after ISC; 10% of addition occurs at the central carbon in propyne, whereas 89% occurs at the terminal carbon.

With this work, product formation and the extent of ISC have now been explored for the reaction of $O(^3P)$ with all linear unsaturated two- and three-carbon species, albeit with variations in the initial conditions (thermal vs single collision). Current work is underway investigating the reaction of $O(^3P)$ with larger-chain unsaturated hydrocarbons and species with other bonding motifs (e.g., unsaturated cyclic hydrocarbons), and also studies that quantitatively probe the products of $O(^3P)$ + propyne at a variety of different conditions (e.g., temperature and pressure).

■ ASSOCIATED CONTENT

Supporting Information

Description of the kinetics model, absolute photoionization cross-section measurements, evaluation of the methylketenyl photoionization cross-section, additional description of the assignment of primary and secondary products, evaluated energetics for the decomposition of C_2H_4, description of the hydrogen scrambling mechanism on the C_3H_4O potential energy surface, and calculated energetics for $C_3H_3O^+$ species. The Supporting Information is available free of charge on the ACS Publications website at DOI: 10.1021/acs.jpca.5b00491.

■ AUTHOR INFORMATION

Corresponding Author

*E-mail: dlosbor@sandia.gov. Tel: (925) 294-4622.

Present Address

§O.W.: Institute for Combustion and Gas Dynamics, University of Duisburg-Essen, Duisburg, Germany

Notes

The authors declare no competing financial interest.

■ ACKNOWLEDGMENTS

We thank Mr. Howard Johnsen and the staff of the Chemical Dynamics Beamline at the Advanced Light Source for technical support of these experiments. This material is based upon work supported by the U.S. Department of Energy Office of Science, Office of Basic Energy Sciences. Sandia is a multi-program

DOI: 10.1021/acs.jpca.5b00491
J. Phys. Chem. A 2015, 119, 7388−7403

laboratory operated by Sandia Corporation, a Lockheed Martin Company, for the National Nuclear Security Administration under contract no. DE-AC04-94-AL85000. This research used resources of the Advanced Light Source, a DOE Office of Science User Facility, which is supported by the Director, Office of Science, Office of Basic Energy Sciences, the U.S. Department of Energy under contract no. DE-AC02-05CH11231 at Lawrence Berkeley National Laboratory.

REFERENCES

(1) Miller, J. A.; Kee, R. J.; Westbrook, C. K. Chemical Kinetics and Combustion Modeling. *Annu. Rev. Phys. Chem.* **1990**, *41*, 345−387.
(2) Cvetanovic, R. J.; Singleton, D. L. Reaction of Oxygen Atoms with Olefins. *Rev. Chem. Int.* **1984**, *5*, 183−226.
(3) Cvetanovic, R. J. Evaluated Chemical Kinetic Data for the Reactions of Atomic Oxygen $O(^3P)$ with Unsaturated Hydrocarbons. *J. Phys. Chem. Ref. Data* **1987**, *16*, 261−326.
(4) Capozza, G.; Segoloni, E.; Leonori, F.; Volpi, G. G.; Casavecchia, P. Soft Electron Impact Ionization in Crossed Molecular Beam Reactive Scattering: The Dynamics of the $O(^3P)+C_2H_2$ Reaction. *J. Chem. Phys.* **2004**, *120*, 4557−4560.
(5) Leonori, F.; Balucani, N.; Capozza, G.; Segoloni, E.; Volpi, G. G.; Casavecchia, P. Dynamics of the $O(^3P)+C_2H_2$ Reaction From Crossed Molecular Beam Experiments with Soft Electron Ionization Detection. *Phys. Chem. Chem. Phys.* **2014**, *16*, 10008−10022.
(6) Casavecchia, P.; Capozza, G.; Segoloni, E.; Leonori, F.; Balucani, N.; Volpi, G. G. Dynamics of the $O(^3P)+C_2H_4$ Reaction: Identification of Five Primary Product Channels (Vinoxy, Acetyl, Methyl, Methylene, and Ketene) and Branching Ratios by the Crossed Molecular Beam Technique with Soft Electron Ionization. *J. Phys. Chem. A* **2005**, *109*, 3527−3530.
(7) Lee, S. H.; Huang, W. J.; Chen, W. K. Dynamics of the Reaction of Atomic Oxygen with Ethene: Observation of All Carbon-Containing Products by Single-Photon Ionization. *Chem. Phys. Lett.* **2007**, *446*, 276−280.
(8) Lee, S. H.; Chen, W. K.; Huang, W. J. Exploring the Dynamics of Reactions of Oxygen Atoms in States ^3P and ^1D with Ethene at Collision Energy 3 kcal mol^{-1}. *J. Chem. Phys.* **2009**, *130*, No. 054301.
(9) Leonori, F.; Occhiogrosso, A.; Balucani, N.; Bucci, A.; Petrucci, R.; Casavecchia, P. Crossed Molecular Beam Dynamics Studies of the $O(^3P)$ + Allene Reaction: Primary Products, Branching Ratios, and Dominant Role of Intersystem Crossing. *J. Phys. Chem. Lett.* **2012**, *3*, 75−80.
(10) Balucani, N.; Leonori, F.; Nevrly, V.; Falcinelli, S.; Bergeat, A.; Stranges, D.; Casavecchia, P. Reaction Dynamics and Relative Yields of the H- and CH_3-Displacement Channels in the O + CH_3CCH Reaction. *Chem. Phys. Lett.* **2014**, *602*, 58−62.
(11) Nguyen, T. L.; Vereecken, L.; Peeters, J. Quantum Chemical and Theoretical Kinetics Study of the $O(^3P)+C_2H_2$ Reaction: A Multistate Process. *J. Phys. Chem. A* **2006**, *110*, 6696−6706.
(12) Nguyen, T. L.; Vereecken, L.; Hou, X. J.; Nguyen, M. T.; Peeters, J. Potential Energy Surfaces, Product Distributions and Thermal Rate Coefficients of the Reaction of $O(^3P)$ with $C_2H_4(X^1A_g)$: A Comprehensive Theoretical Study. *J. Phys. Chem. A* **2005**, *109*, 7489−7499.
(13) Nguyen, T. L.; Peeters, J.; Vereecken, L. Quantum Chemical and Statistical Rate Study of the Reaction of $O(^3P)$ with Allene: O-Addition and H-Abstraction Channels. *J. Phys. Chem. A* **2006**, *110*, 12166−12176.
(14) Hu, W.; Lendvay, G.; Maiti, B.; Schatz, G. C. Trajectory Surface Hopping Study of the $O(^3P)$ Plus Ethylene Reaction Dynamics. *J. Phys. Chem. A* **2008**, *112*, 2093−2103.
(15) Fu, B. N.; Han, Y. C.; Bowman, J. M.; Angelucci, L.; Balucani, N.; Leonori, F.; Casavecchia, P. Intersystem Crossing and Dynamics in $O(^3P)+C_2H_4$ Multichannel Reaction: Experiment Validates Theory. *Proc. Natl. Acad. Sci. U.S.A.* **2012**, *109*, 9733−9738.
(16) Rajak, K.; Maiti, B. Communications: Direct Dynamics Study of the $O(^3P)+C_2H_2$ Reaction: Contribution From Spin Nonconserving Route. *J. Chem. Phys.* **2010**, *133*, No. 011101.
(17) Fu, B.; Han, Y. C.; Bowman, J. M.; Leonori, F.; Balucani, N.; Angelucci, L.; Occhiogrosso, A.; Petrucci, R.; Casavecchia, P. Experimental and Theoretical Studies of the $O(^3P)+C_2H_4$ Reaction Dynamics: Collision Energy Dependence of Branching Ratios and Extent of Intersystem Crossing. *J. Chem. Phys.* **2012**, *137*, No. 22A532.
(18) Taatjes, C. A.; Osborn, D. L.; Selby, T. M.; Meloni, G.; Trevitt, A. J.; Epifanovsky, E.; Krylov, A. I.; Sirjean, B.; Dames, E.; Wang, H. Products of the Benzene+$O(^3P)$ Reaction. *J. Phys. Chem. A* **2010**, *114*, 3355−3370.
(19) Savee, J. D.; Welz, O.; Taatjes, C. A.; Osborn, D. L. New Mechanistic Insights to the $O(^3P)$+Propene Reaction From Multiplexed Photoionization Mass Spectrometry. *Phys. Chem. Chem. Phys.* **2012**, *14*, 10410−10423.
(20) Kanofsky, J. R.; Lucas, D.; Pruss, F.; Gutman, D. Direct Identification of Reactive Channels in Reactions of Oxygen Atoms and Hydroxyl Radicals with Acetylene and Methylacetylene. *J. Phys. Chem.* **1974**, *78*, 311−316.
(21) Zhao, S. L.; Wu, W. Q.; Zhao, H. M.; Wang, H.; Yang, C. F.; Liu, K. H.; Su, H. M. Adiabatic and Nonadiabatic Reaction Pathways of the $O(^3P)$ with Propyne. *J. Phys. Chem. A* **2009**, *113*, 23−34.
(22) Chin, C. H.; Lee, S. H. Theoretical Study of Isomerization and Decomposition of Propenal. *J. Chem. Phys.* **2011**, *134*, No. 044309.
(23) Osborn, D. L.; Zou, P.; Johnsen, H.; Hayden, C. C.; Taatjes, C. A.; Knyazev, V. D.; North, S. W.; Peterka, D. S.; Ahmed, M.; Leone, S. R. The Multiplexed Chemical Kinetic Photoionization Mass Spectrometer: A New Approach to Isomer-Resolved Chemical Kinetics. *Rev. Sci. Instrum.* **2008**, *79*, No. 104103.
(24) Savee, J. D.; Soorkia, S.; Welz, O.; Selby, T. M.; Taatjes, C. A.; Osborn, D. L. Absolute Photoionization Cross-Section of the Propargyl Radical. *J. Chem. Phys.* **2012**, *136*, No. 134307.
(25) Taatjes, C. A.; Hansen, N.; Osborn, D. L.; Kohse-Hoinghaus, K.; Cool, T. A.; Westmoreland, P. R. "Imaging" Combustion Chemistry via Multiplexed Synchrotron-Photoionization Mass Spectrometry. *Phys. Chem. Chem. Phys.* **2008**, *10*, 20−34.
(26) Heimann, P. A.; Koike, M.; Hsu, C. W.; Blank, D.; Yang, X. M.; Suits, A. G.; Lee, Y. T.; Evans, M.; Ng, C. Y.; Flaim, C.; et al. Performance of the Vacuum Ultraviolet High-Resolution and High-Flux Beamline for Chemical Dynamics Studies at the Advanced Light Source. *Rev. Sci. Instrum.* **1997**, *68*, 1945−1951.
(27) Leone, S. R.; Ahmed, M.; Wilson, K. R. Chemical Dynamics, Molecular Energetics, and Kinetics at the Synchrotron. *Phys. Chem. Chem. Phys.* **2010**, *12*, 6564−6578.
(28) Arrington, C. A.; Cox, D. J. Arrhenius Parameters for Reaction of Oxygen Atoms, $O(^3P)$, with Propyne. *J. Phys. Chem.* **1975**, *79*, 2584−2586.
(29) Aleksandrov, E. N.; Dubrovina, I. V.; Kozlov, S. N. The Reaction of Oxygen Atoms with Methylacetylene. *Kinet. Catal.* **1981**, *22*, 394−396.
(30) Homann, K. H.; Wellmann, C. Kinetics and Mechanisms of Hydrocarbon Formation in the System C_2H_2/O/H at Temperatures up to 1300 K. *Ber. Bunsen-Ges. Phys. Chem. Chem. Phys.* **1983**, *87*, 609−616.
(31) Adusei, G. Y.; Blue, A. S.; Fontijn, A. The $O(^3P)$ Methylacetylene Reaction Over Wide Temperature and Pressure Ranges. *J. Phys. Chem.* **1996**, *100*, 16921−16924.
(32) Estupiñán, E. G.; Nicovich, J. M.; Wine, P. H. A Temperature-Dependent Kinetics Study of the Important Stratospheric Reaction $O(^3P)+NO_2\leftrightarrow O_2+NO$. *J. Phys. Chem. A* **2001**, *105*, 9697−9703.
(33) Gierczak, T.; Burkholder, J. B.; Ravishankara, A. R. Temperature Dependent Rate Coefficient for the Reaction $O(^3P)+NO_2\leftrightarrow NO+O_2$. *J. Phys. Chem. A* **1999**, *103*, 877−883.
(34) Vandaele, A. C.; Hermans, C.; Simon, P. C.; Carleer, M.; Colin, R.; Fally, S.; Merienne, M. F.; Jenouvrier, A.; Coquart, B. Measurements of the NO_2 Absorption Cross-Section From 42000 cm^{-1} to 10000 cm^{-1} (238−1000 nm) at 220 and 294 K. *J. Quant. Spectrosc. Radiat. Transfer* **1998**, *59*, 171−184.

DOI: 10.1021/acs.jpca.5b00491
J. Phys. Chem. A 2015, 119, 7388−7403

(35) Sander, S. P.; Abbatt, J.; Barker, J. R.; Burkholder, J. B.; Friedl, R. R.; Golden, D. M.; Huie, R. E.; Kolb, C. E.; Kurylo, M. J.; Moortgat, G. K.; et al. Chemical Kinetics and Photochemical Data for Use in Atmospheric Studies, Evaluation No. 17. JPL Publication 10-6; Jet Propulsion Laboratory: Pasadena, 2011.
(36) Lias, S. G. Ionization Energy Evaluation. In *NIST Chemistry WebBook*, NIST Standard Reference Database Number 69; Linstrom, P. J., Mallard, W. G., Eds.; National Institute of Standards and Technology: Gaithersburg, MD.
(37) Cool, T. A.; McIlroy, A.; Qi, F.; Westmoreland, P. R.; Poisson, L.; Peterka, D. S.; Ahmed, M. Photoionization Mass Spectrometer for Studies of Fame Chemistry with a Synchrotron Light Source. *Rev. Sci. Instrum.* **2005**, *76*, No. 094102.
(38) Welz, O.; Zádor, J.; Savee, J. D.; Ng, M. Y.; Meloni, G.; Fernandes, R. X.; Sheps, L.; Simmons, B. A.; Lee, T. S.; Osborn, D. L.; et al. Low Temperature Combustion Chemistry of Biofuels: Pathways in the Initial Low-Temperature (550 K−750 K) Oxidation Chemistry of Isopentanol. *Phys. Chem. Chem. Phys.* **2012**, *14*, 3112−3127.
(39) Montgomery, J. A.; Frisch, M. J.; Ochterski, J. W.; Petersson, G. A. A Complete Basis Set Model Chemistry. VI. Use of Density Functional Geometries and Frequencies. *J. Chem. Phys.* **1999**, *110*, 2822−2827.
(40) Montgomery, J. A.; Frisch, M. J.; Ochterski, J. W.; Petersson, G. A. A Complete Basis Set Model Chemistry. VII. Use of the Minimum Population Localization Method. *J. Chem. Phys.* **2000**, *112*, 6532−6542.
(41) Frisch, M. J.; Trucks, G. W.; Schlegel, H. B.; Scuseria, G. E.; Robb, M. A.; Cheeseman, J. R.; Scalmani, G.; Barone, V.; Mennucci, B.; Petersson, G. A.; et al. *Gaussian 09*, Revision B.01; Gaussian, Inc.: Wallingford, CT, 2009.
(42) McKellar, A. R. W.; Bunker, P. R.; Sears, T. J.; Evenson, K. M.; Saykally, R. J.; Langhoff, S. R. Far Infrared Laser Magnetic Resonance of Singlet Methylene−Singlet Triplet Perturbations, Singlet Triplet Transitions, and the Singlet Triplet Splitting. *J. Chem. Phys.* **1983**, *79*, 5251−5264.
(43) Kanofsky, J. R.; Gutman, D. Direct Observation of Products Produced by O-Atom Reactions with Ethylene and Propylene Studied in High-Intensity Molecular Beams. *Chem. Phys. Lett.* **1972**, *15*, 236−ff.
(44) Savee, J. D.; Lockyear, J. F.; Borkar, S.; Eskola, A. J.; Welz, O.; Taatjes, C. A.; Osborn, D. L. Absolute Photoionization Cross-Section of the Vinyl Radical. *J. Chem. Phys.* **2013**, *139*, No. 056101.
(45) Lago, A. F.; Baer, T. A Photoelectron Photoion Coincidence Study of the Vinyl Bromide and Tribromoethane Ion Dissociation Dynamics: Heats of Formation of $C_2H_3^+$, $C_2H_3Br^+C_2H_3Br^+$, $C_2H_3Br_2^+$, and $C_2H_3Br_3$. *J. Phys. Chem. A* **2006**, *110*, 3036−3041.
(46) Ervin, K. M.; Gronert, S.; Barlow, S. E.; Gilles, M. K.; Harrison, A. G.; Bierbaum, V. M.; Depuy, C. H.; Lineberger, W. C.; Ellison, G. B. Bond Strengths of Ethylene and Acetylene. *J. Am. Chem. Soc.* **1990**, *112*, 5750−5759.
(47) Quandt, R.; Min, Z. Y.; Wang, X. B.; Bersohn, R. Reactions of $O(^3P)$ with Alkenes: H, CH_2CHO, CO, and OH Channels. *J. Phys. Chem. A* **1998**, *102*, 60−64.
(48) Riedel, J.; Dziarzhytski, S.; Kuczmann, A.; Renth, F.; Temps, F. Velocity Map Ion Imaging of H Atoms from the Dissociation of HCO (A^2A'') Using Doppler-Free Multi-Photon Ionization. *Chem. Phys. Lett.* **2005**, *414*, 473−478.
(49) Berkowitz, J.; Ellison, G. B.; Gutman, D. Three Methods to Measure RH Bond Energies. *J. Phys. Chem.* **1994**, *98*, 2744−2765.
(50) Taatjes, C. A.; Osborn, D. L.; Selby, T. M.; Meloni, G.; Fan, H. Y.; Pratt, S. T. Absolute Photoionization Cross-Section of the Methyl Radical. *J. Phys. Chem. A* **2008**, *112*, 9336−9343.
(51) Lias, S. G.; J.E, B.; Liebman, J. F.; Holmes, J. L.; R.D, L.; Mallard, W. G. Gas-Phase Ion and Neutral Thermochemistry. *J. Phys. Chem. Ref. Data* **1988**, *17*, 1−861.
(52) Casavecchia, P.; Leonori, F.; Balucani, N.; Petrucci, R.; Capozza, G.; Segoloni, E. Probing the Dynamics of Polyatomic Multichannel Elementary Reactions by Crossed Molecular Beam Experiments with Soft Electron-Ionization Mass Spectrometric Detection. *Phys. Chem. Chem. Phys.* **2009**, *11*, 46−65.
(53) Gans, B.; Mendes, L. A. V.; Boye-Peronne, S.; Douin, S.; Garcia, G.; Soldi-Lose, H.; de Miranda, B. K. C.; Alcaraz, C.; Carrasco, N.; Pernot, P.; et al. Determination of the Absolute Photoionization Cross Sections of CH_3 and I Produced from a Pyrolysis Source, by Combined Synchrotron and Vacuum Ultraviolet Laser Studies. *J. Phys. Chem. A* **2010**, *114*, 3237−3246.
(54) Loison, J. C. Absolute Photoionization Cross Section of the Methyl Radical. *J. Phys. Chem. A* **2010**, *114*, 6515−6520.
(55) Xing, G. Q.; Huang, X.; Wang, X. B.; Bersohn, R. Reactions of $O(^3P)$ with Alkynes: The CO and H Atom Channels. *J. Chem. Phys.* **1996**, *105*, 488−495.
(56) Chin, C. H.; Chaudhuri, C.; Lee, S. H. Molecular-Beam Experiments for Photodissociation of Propenal at 157 nm and Quantum-Chemical Calculations for Migration and Elimination of Hydrogen Atoms in Systems C_3H_4O and C_3H_3O. *J. Chem. Phys.* **2011**, *135*, No. 044301.
(57) Bobeldijk, M.; Vanderzande, W. J.; Kistemaker, P. G. Simple Models for the Calculation of Photoionization and Electron Impact Ionization Cross-Sections of Polyatomic Molecules. *Chem. Phys.* **1994**, *179*, 125−130.
(58) Lin, M. C.; Shortridge, R. G.; Umstead, M. E. Dynamics of Reactions of $O(^3P)$ Atoms with Allene and Methylacetylene. *Chem. Phys. Lett.* **1976**, *37*, 279−284.
(59) Umstead, M. E.; Shortridge, R. G.; Lin, M. C. Dynamics of CO Production from $O(^3P)$+Methylacetylene Reaction. *Chem. Phys.* **1977**, *20*, 271−276.
(60) Nguyen, M. T.; Matus, M. H.; Lester, W. A.; Dixon, D. A. Heats of Formation of Triplet Ethylene, Ethylidene, and Acetylene. *J. Phys. Chem. A* **2008**, *112*, 2082−2087.
(61) Jacovella, U.; Gans, B.; Merkt, F. On the Adiabatic Ionization Energy of the Propargyl Radical. *J. Chem. Phys.* **2013**, *139*, No. 084308.
(62) Vereecken, L.; Pierloot, K.; Peeters, J. B3LYP-DFT Characterization of the Potential Energy Surface of the $CH(X^2\Pi)+C_2H_2$ Reaction. *J. Chem. Phys.* **1998**, *108*, 1068−1080.
(63) Xu, H.; Pratt, S. T. Photoionization Cross Section of the Propargyl Radical and Some General Ideas for Estimating Radical Cross Sections. *J. Phys. Chem. A* **2013**, *117*, 9331−9342.
(64) McNaughton, D.; Suffolk, R. J. The Production and Photoelectron Spectrum of Propa-1,2-dien-3-one, C_3H_2O. *J. Chem. Res.-S* **1985**, 32−32.
(65) Terlouw, J. K.; Holmes, J. L.; Lossing, F. P. Ionized Ethylidene Ketene and its Homolog Methylene Ketene. *Can. J. Chem.-Rev. Can. Chim.* **1983**, *61*, 1722−1724.
(66) Opitz, J. Photoionization of Propynal in the Gas-Phase. *Int. J. Mass Spectrom. Ion Process* **1991**, *107*, 503−513.
(67) Vonniessen, W.; Bieri, G.; Asbrink, L. 30.4 nm He(II) Photoelectron Spectra of Organic Molecules 3. Oxo-Compounds (C,H,O). *J. Electron Spectrosc. Relat. Phenom.* **1980**, *21*, 175−191.
(68) Carlier, P.; Mouvier, G. Spectrometric Study of Photoelectrons of Electronic Structure of Conjugated Ynals and Ynones. *J. Electron Spectrosc. Relat. Phenom.* **1979**, *17*, 169−180.
(69) Zhang, W.; Du, B.; Feng, C. Ab Initio Dynamics Study on the Reaction of $O(^3P)$ with $CH_3CH{=}CH_2$ ($^1A'$). *J. Mol. Struct.* **2007**, *806*, 121−129.
(70) West, A. C.; Kretchmer, J. S.; Sellner, B.; Park, K.; Hase, W. L.; Lischka, H.; Windus, T. L. $O(^3P)$ + C_2H_4 Potential Energy Surface: Study at the Multireference Level. *J. Phys. Chem. A* **2009**, *113*, 12663−12674.
(71) DeBoer, G. D.; Dodd, J. A. Ab Initio Energies and Product Branching Ratios for the $O+C_3H_6$ Reaction. *J. Phys. Chem. A* **2007**, *111*, 12977−12984.
(72) Lee, S. H.; Chin, C. H.; Chaudhuri, C. Evidence for Synchronous Concerted Three-Body Dissociation of Propenal to $C_2H_2+CO+H_2$. *ChemPhysChem* **2011**, *12*, 753−756.
(73) Chaudhuri, C.; Lee, S. H. A Complete Look at the Multi-Channel Dissociation of Propenal Photoexcited at 193 nm: Branching Ratios and Distributions of Kinetic Energy. *Phys. Chem. Chem. Phys.* **2011**, *13*, 7312−7321.

DOI: 10.1021/acs.jpca.5b00491
J. Phys. Chem. A 2015, 119, 7388−7403

(74) Heazlewood, B. R.; Maccarone, A. T.; Andrews, D. U.; Osborn, D. L.; Harding, L. B.; Klippenstein, S. J.; Jordan, M. J. T.; Kable, S. H. Near-Threshold H/D Exchange in CD_3CHO Photodissociation. *Nat. Chem.* **2011**, *3*, 443−448.

DOI: 10.1021/acs.jpca.5b00491
J. Phys. Chem. A 2015, 119, 7388−7403